Computers & Geosciences 90 (2016) 24–39

Contents lists available at ScienceDirect

Computers & Geosciences

journal homepage: www.elsevier.com/locate/cageo

Case study

Shelf sediment transport during hurricanes Katrina and Rita

Kehui Xu [a,b,*], Rangley C. Mickey [c], Qin Chen [b,d,e], Courtney K. Harris [f], Robert D. Hetland [g], Kelin Hu [e], Jiaze Wang [a,b]

[a] Department of Oceanography and Coastal Sciences, Louisiana State University, Baton Rouge, LA 70803, USA
[b] Coastal Studies Institute, Louisiana State University, Baton Rouge, LA 70803, USA
[c] Cherokee Nation Technologies contracted to the U.S. Geological Survey, USA
[d] Department of Civil and Environmental Engineering, Louisiana State University, Baton Rouge, LA 70803, USA
[e] Center for Computation and Technology, Louisiana State University, Baton Rouge, LA 70803, USA
[f] Virginia Institute of Marine Science, College of William & Mary, Gloucester Point, VA 23062, USA
[g] Department of Oceanography, Texas A&M University, College Station, TX 77843, USA

ARTICLE INFO

Article history:
Received 29 January 2015
Received in revised form
13 October 2015
Accepted 14 October 2015
Available online 19 October 2015

Keywords:
Sediment transport
Numerical model
Hurricanes Katrina and Rita
Seabed erodibility
Erosional rate
Settling velocity

ABSTRACT

Hurricanes can greatly modify the sedimentary record, but our coastal scientific community has rather limited capability to predict hurricane-induced sediment deposition. A three-dimensional sediment transport model was developed in the Regional Ocean Modeling System (ROMS) to study seabed erosion and deposition on the Louisiana shelf in response to Hurricanes Katrina and Rita in the year 2005. Sensitivity tests were performed on both erosional and depositional processes for a wide range of erosional rates and settling velocities, and uncertainty analysis was done on critical shear stresses using the polynomial chaos approximation method. A total of 22 model runs were performed in sensitivity and uncertainty tests. Estimated maximum erosional depths were sensitive to the inputs, but horizontal erosional patterns seemed to be controlled mainly by hurricane tracks, wave–current combined shear stresses, seabed grain sizes, and shelf bathymetry. During the passage of two hurricanes, local resuspension and deposition dominated the sediment transport mechanisms. Hurricane Katrina followed a shelf-perpendicular track before making landfall and its energy dissipated rapidly within about 48 h along the eastern Louisiana coast. In contrast, Hurricane Rita followed a more shelf-oblique track and disturbed the seabed extensively during its 84-h passage from the Alabama–Mississippi border to the Louisiana–Texas border. Conditions to either side of Hurricane Rita's storm track differed substantially, with the region to the east having stronger winds, taller waves and thus deeper erosions. This study indicated that major hurricanes can disturb the shelf at centimeter to meter levels. Each of these two hurricanes suspended seabed sediment mass that far exceeded the annual sediment inputs from the Mississippi and Atchafalaya Rivers, but the net transport from shelves to estuaries is yet to be determined. Future studies should focus on the modeling of sediment exchange between estuaries and shelves and the field measurement of erosional rates and settling velocities.

1. Introduction

Episodic events, such as river floods and hurricanes, happen over a relatively short period of time (hours to weeks), but can greatly modify the sedimentary record. However, our coastal scientific community has rather limited ability to predict the characteristics of strata produced by even well-observed modern-day events (Corbett et al., 2014). This is probably due to either the lack of field measurements or the damage of optical and acoustic sensors during energetic and extreme events.

It is well known that hurricanes drive energetic winds and generate currents and waves, both propagating toward the land. When the hurricanes reach continental shelves, seabed sediment is suspended to water column, causing the erosion on seabed. The seabed elevation difference between pre-hurricane level and the "deepest cut" is thus defined as "maximum erosional depth" (Fig. 1A), which is also called "bed scour" (Keen and Glenn, 2002). After making landfalls, hurricanes dissipate and sediment settles back to seabed or in coastal estuaries and wetlands. The seabed elevation difference between the deepest cut and post-hurricane level is thus defined as "post-hurricane deposit" (Fig. 1A and B). Net erosion/deposition is defined as the difference between pre- and post-hurricane levels. During the passage of hurricanes, some

* Corresponding author at: Department of Oceanography and Coastal Sciences, Louisiana State University, 2165 Energy, Coast and Environment Building, Baton Rouge, LA 70803, USA.
E-mail address: kxu@lsu.edu (K. Xu).

http://dx.doi.org/10.1016/j.cageo.2015.10.009
0098-3004/

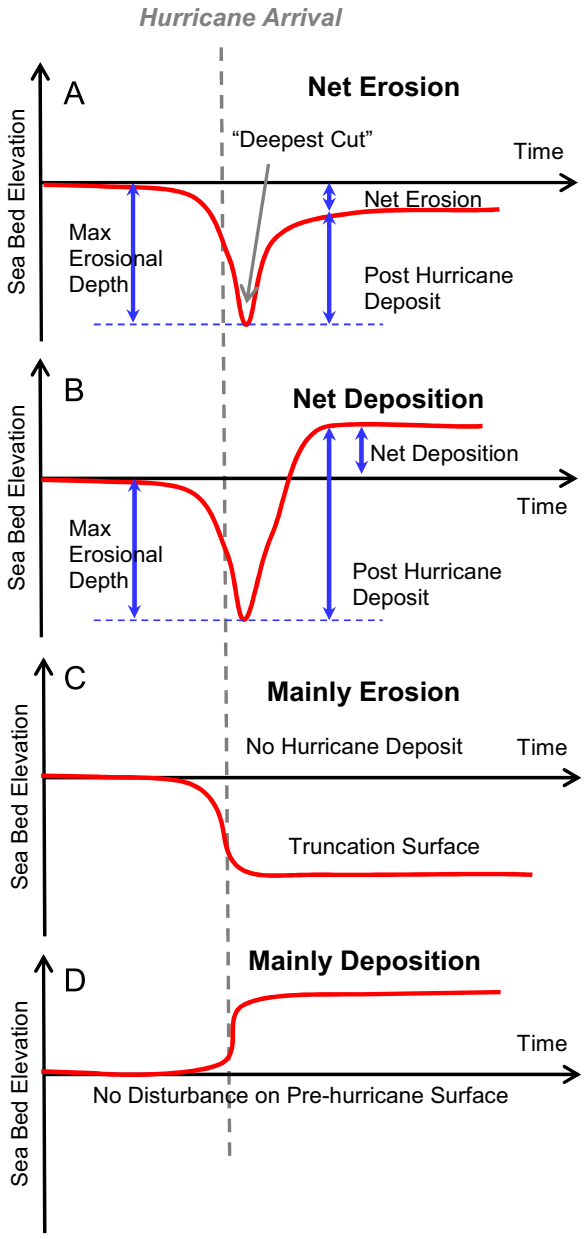

Fig. 1. Conceptual diagrams of four types of sea bed elevation changes during and after the arrival of a hurricane. Maximum erosional depth is defined as the change between pre-hurricane seabed surface and the "deepest cut" during the peak of a hurricane, and is also called bed scour. Post-hurricane deposition represents the difference between the sea bed elevation after the storm and the peak erosion during the storm. Net erosion or deposition represents the difference between the post-hurricane and pre-hurricane sea bed levels.

regions may experience erosion only (Fig. 1C), whereas other areas like costal bays/wetlands may have deposition only (Fig. 1D). Turner et al. (2006) reported that the major source of mineral sediment to Louisiana coastal marshes is from hurricanes, not river floods. Törnqvist et al. (2007), however, believed that there were an over-estimation of hurricane return periods and a lack of erosion measurements in the study of Turner et al. (2006). By now our coastal scientific community has not reached a consensus on sediment dynamics during hurricanes. No matter if rivers or hurricanes play a more important role in wetland sedimentation, it is the *net erosion/deposition* that actually impacts sediment budget, not the post-hurricane deposition, as shown in Fig. 1. Unfortunately it is well known that the erosional process is challenging to measure in sedimentary system. In some environments erosion can be measured using either the comparisons among repeated field surveys (e.g., Goff et al., 2010) or the numerical models (e.g., Xu et al., 2011).

In this study we focus on Louisiana continental shelf sediment transport during hurricanes. Hurricanes strike the Louisiana coast approximately once every three years, normally between May and November (Neumann et al., 1993). Based on an overview of hurricane impacts, Stone et al. (1997) found that hurricanes cause chronic erosion to Louisiana barrier systems, but sometime also generate considerable deposition in Louisiana's marshes and bays. They also reported that Hurricanes Audrey (1957) and Andrew (1992) formed 0.70 and 0.16 m of mixed organic and inorganic debris in Louisiana marsh areas, respectively. Goni et al. (2006) collected sediment samples in the inner shelf southwest of Atchafalaya Bay after Hurricane Lili (2002) and identified a storm layer up to 0.2 m thick; they also found fining-upward deposits to be composed of silty clays with a sandy basal layer. Keen and Glenn (2002) predicted bed scour on the continental shelf during Hurricane Andrew (1992) and simulated storm sedimentation on the sandy Ship Shoal (Fig. 2) of Louisiana shelf; they found that the bottom boundary layer was wave-dominated and bed scour was primarily by resuspension. Goff et al. (2010) found offshore sediment transport during Hurricane Ike (2008) and believed that shoreface sands appear to have been incised by the storm and advected offshore by the strong storm-surge ebb currents.

In this study we focus on Hurricanes Katrina and Rita, both of which happened in the year 2005. The economic and environmental damages caused by Katrina were over $40 billion of insured losses (Knabb et al., 2006). Hurricane Katrina formed as a tropical depression on August 23, 2005 over the Bahamas Islands. After passing the southern tip of Florida, it moved westward into the Gulf of Mexico where it gained strength to become a category five hurricane in August 28. Then it swept northward and made landfall on August 29 over the Mississippi River Delta (MRD) as a category four hurricane (http://www.csc.noaa.gov; Fig. 2). About three weeks later, Hurricane Rita formed as a tropical depression in the Caribbean Sea and headed westward into the Gulf of Mexico. On September 21 it became a category five hurricane and moved northwest toward the western Louisiana coastline, where it made landfall on September 24 at the Texas–Louisiana border as a category three hurricane (Fig. 2).

Multiple event-response studies have been performed in wetland, estuary and shelf areas after Hurricanes Katrina and Rita. Turner et al. (2006), for example, reported that more than 131 Million Tons (Mt) of post-hurricane sediment deposited in coastal wetlands when Hurricanes Katrina and Rita crossed the Louisiana coast; they identified several cm thick of sediment deposition on wetlands. Based on further data analyses, Tweel and Turner (2012) reported that sediment deposition on coastal wetlands was 68 and 48 Mt from Hurricanes Katrina and Rita, respectively. Using gain size, X-radiographs, and gamma-density data for sediment cores, Keen et al. (2006) found that Hurricane Katrina deposited a storm bed east of landfall on the Louisiana shelf with a maximum observed thickness of 0.58 m, which thinned to approximately 0.1 m about 200 km west of landfall; they also reported that the fining-upward bed is similar to event beds observed in both ancient and modern sedimentary environments. Based on a collaborative multi-institution rapid-response effort, Walsh et al. (2006) collected bathymetric and sediment core data in the MRD and reported the evidence of mud flow activities near the Mississippi subaqueous delta after two hurricanes. Goni et al. (2007) studied radionuclides, x-radiographs and stable isotopes by analyzing 1-cm thick slices in post-hurricane Katrina/Rita deposits and found that the post-hurricane layers was predominantly local sediments mobilized by the intense wave activity during the storms; they also believed that post-hurricane deposit thicknesses ranged

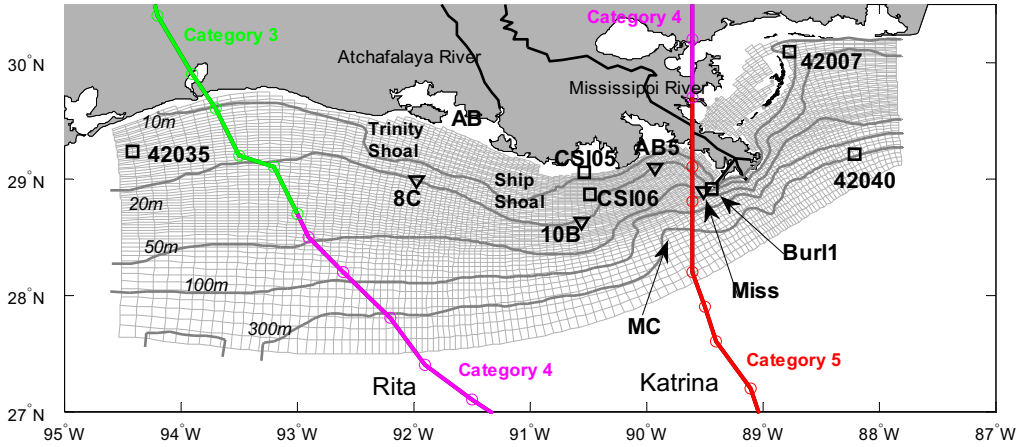

Fig. 2. The curvilinear model grid used for the Louisiana–Texas shelf. Isobaths contoured at water depths of 10, 20, 50, 100, and 300 m, and used throughout this entire paper. Squares are observational stations maintained by NOAA National Data Buoy Center (NDBC) as well as Louisiana State University's Wave–Current–Surge Information System (WAVCIS) system. Three triangles of 8C, 10B and AB5 are stations used from hypoxia studies along the 20-m isobaths; Station Miss is used to study the change right offshore of the Mississippi Delta. AB=Atchafalaya Bay; MRD=Mississippi River Delta; MC=Mississippi Canyon. Color lines and circles show the tracks of Hurricanes Katrina and Rita; red, purple and green correspond category 5, 4 and 3 of hurricanes, respectively. (For interpretation of the references to color in this figure legend, the reader is referred to the web version of this article.)

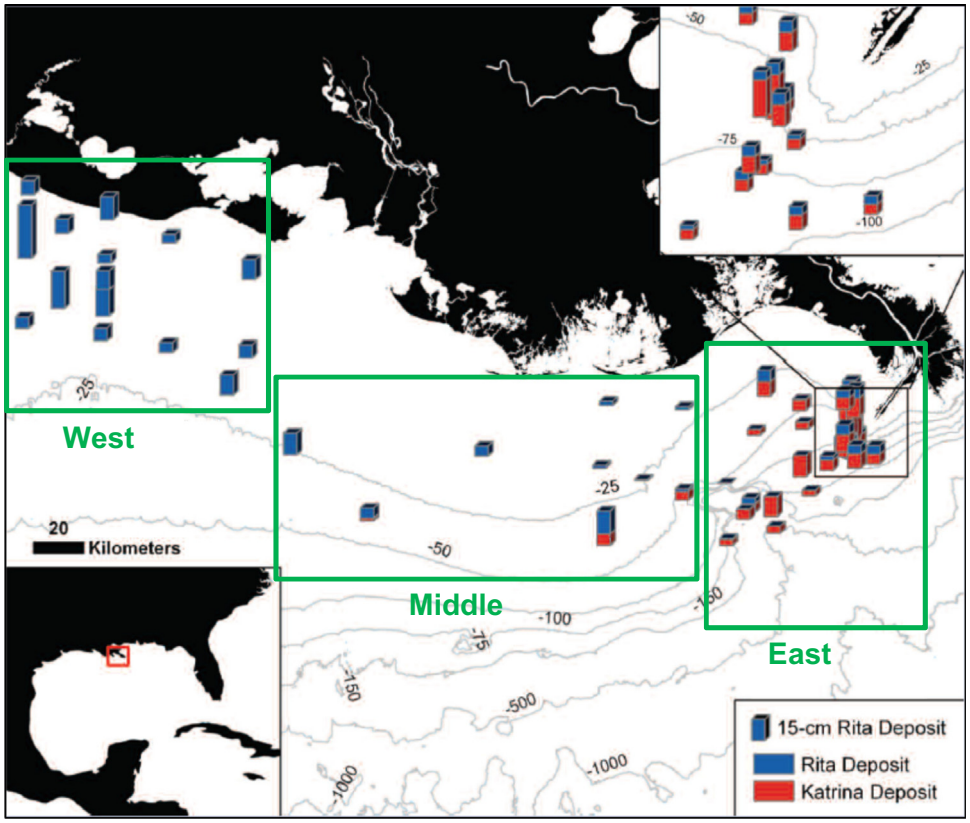

Fig. 3. Map illustrating the thickness of sediment deposits associated with Hurricanes Katrina and Rita (from Goni et al. (2007)). Deposit data are mainly based on radionuclide and x-radiographic analyses in 41 sediment cores. Three areas are defined: west, middle and east. Detailed comparison of three areas can be found in Tables 2 and 3.

from centimeter to decimeter levels (Fig. 3).

2. Motivations and objectives

Despite the above extensive research efforts, 3-D hurricane sediment transport modeling studies are rather limited for Louisiana shelf. Surprisingly the only *3-D hurricane sediment transport* modeling work published so far for Louisiana shelf has been Keen and Glenn (2002), which focused on regional sediment transport at the sandy Ship Shoal during Hurricane Andrew. Xu et al. (2011) developed a 3-D hydrodynamic-sediment transport model for the Texas–Louisiana shelf using the Regional Ocean Modeling System, but the Gulf of Mexico had no hurricanes in the modeled year 1993. They coupled the hydrodynamic model from Hetland and DiMarco (2008) with the Community Sediment Transport Model System (CSTMS) developed by Warner et al. (2008). Both of these modeling efforts, however, relied on model parameters that were difficult to constrain, notably including the erosional rate parameter.

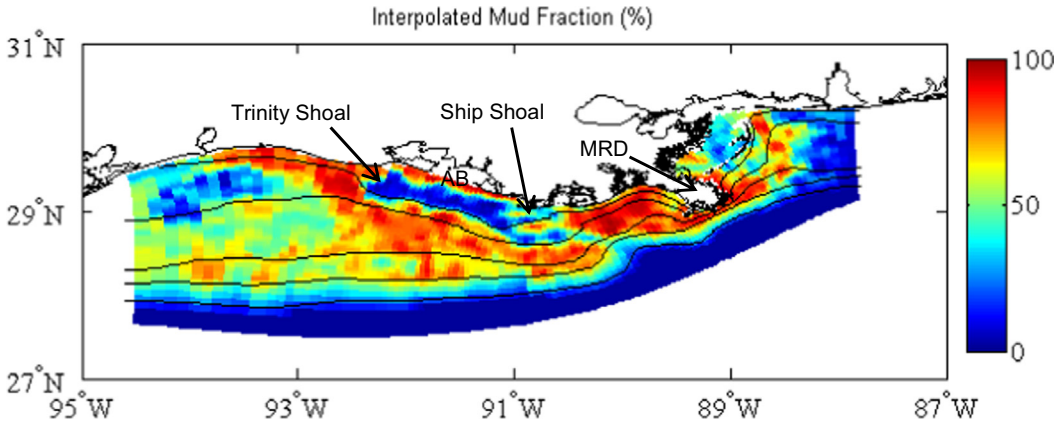

Fig. 4. Interpolated mud fractions based on usSEABED database from Buczkowski et al. (2006). Modified after Fig. 3 in Xu et al. (2011). Sandy Trinity and Ship Shoals are highlighted in the diagram, with essentially no mud. Sandy sediment along southern model edge is used to minimize the boundary effect. AB=Atchafalaya Bay; MRD=Mississippi River Delta.

Table 1
Critical shear stresses (τ_{cr}), settling velocities (W_s) and erosional rate parameter (E_0) used in multiple studies. All these studies used the ROMS sediment transport model.

Study	Area	E_0 (10^{-4} kg/m^2/s)	W_s (mm/s)	τ_{cr} (Pa)
Bever et al. (2009)	Po River Delta	0.5	0.1, 1 and 10	0.03, 0.08, 0.10 and 0.12
Bever and Harris (2014)	Poverty Bay, New Zealand	5	0.038, 0.15. 0.62, 2.4, 10 and 125	0.02, 0.03, 0.06, 0.10, 0.14 and 0.53
Harris et al. (2008)	Adriatic Sea	0.5	0.1, 1 and 10	0.03, 0.08, 0.10 and 0.12
Miles et al. (2015)	Mid-Atlantic Bight	5	5.7 and 52	0.14 and 0.23
Moriarty et al. (2014)	Waipaoa Shelf, New Zealand	0.1 and 4.5	0.1, 0.15, 0.3, 0.5, 1.0 and 125	0.15
Warner et al. (2010)	North Carolina Shelf	Not reported	18	0.17
Xu et al. (2011)	Louisiana Shelf	0.5	0.1, 1 and 10	0.03, 0.08, 0.11 and 0.13
Xue et al. (2012)	Mekong Delta	Not reported	0.1, and 0.25	0.03 and 0.08
This study	Louisiana Shelf	0.5, 1.0, 5.0 and 10.0	0.1, 0.5, 1, 5 and 10	A total of 18 levels from 0.034 to 0.219, listed in Table 2

Table 2
Input and output parameters used in 22 model runs, from R1 to R22. Input parameters include critical shear stresses (τ_{cr}), settling velocities (W_s) and erosional rate parameters (E_0); high and low values of inputs are for fine and coarse seabed sediment tracers, respectively. Output parameters include skills (defined by Willmott (1982)), averages, and standard deviations of modeled post-Rita deposit thicknesses. West, middle and east study areas are defined in Fig. 3. The averages and standard deviations of Goni et al. (2007) study are also shown on top of the table for easier comparison.

Run	E_0	W_s	τ_{cr}	Willmott skill				Average (m)				Standard deviation (m)			
	(10^{-4} kg/m^2/s)	(mm/s)	(Pa)	All	West	Mid	East	All	West	Mid	East	All	West	Mid	East
Goni								*0.086*	*0.137*	*0.061*	*0.055*	*0.071*	*0.085*	*0.058*	*0.026*
R1	0.5	0.1 & 1.0	0.110 & 0.130	0.38	0.42	0.52	0.59	0.033	0.020	0.047	0.037	0.025	0.020	0.027	0.023
R2	1.0	0.1 & 1.0	0.110 & 0.130	0.32	0.45	0.45	0.56	0.060	0.042	0.088	0.062	0.044	0.044	0.050	0.034
R3	5.0	0.1 & 1.0	0.110 & 0.130	0.49	0.63	0.32	0.14	0.194	0.211	0.285	0.132	0.136	0.167	0.117	0.077
R4	10.0	0.1 & 1.0	0.110 & 0.130	0.15	0.20	0.14	0.07	0.627	0.673	0.599	0.601	0.406	0.364	0.348	0.482
R5	0.5	0.5 & 5.0	0.110 & 0.130	0.40	0.40	0.47	0.41	0.005	0.002	0.007	0.006	0.005	0.002	0.006	0.006
R6	1.0	0.5 & 5.0	0.110 & 0.130	0.37	0.40	0.52	0.44	0.020	0.004	0.015	0.036	0.029	0.005	0.014	0.038
R7	5.0	0.5 & 5.0	0.110 & 0.130	0.24	0.41	0.38	0.36	0.052	0.015	0.095	0.062	0.054	0.018	0.062	0.051
R8	10.0	0.5 & 5.0	0.110 & 0.130	0.38	0.42	0.48	0.14	0.096	0.084	0.163	0.072	0.092	0.105	0.105	0.052
R9	0.5	1.0 & 10.0	0.110 & 0.130	0.40	0.40	0.47	0.40	0.002	0.001	0.003	0.004	0.004	0.001	0.003	0.005
R10	1.0	1.0 & 10.0	0.110 & 0.130	0.38	0.40	0.48	0.36	0.011	0.002	0.005	0.022	0.023	0.001	0.006	0.033
R11	5.0	1.0 & 10.0	0.110 & 0.130	0.31	0.40	0.51	0.32	0.039	0.006	0.025	0.075	0.058	0.004	0.024	0.075
R12	10.0	1.0 & 10.0	0.110 & 0.130	0.28	0.41	0.65	0.39	0.047	0.018	0.069	0.062	0.043	0.019	0.049	0.043
R13	2.0	0.1 & 1.0	0.110 & 0.130	0.41	0.53	0.41	0.45	0.101	0.078	0.136	0.102	0.057	0.056	0.066	0.045
R14	3.0	0.1 & 1.0	0.110 & 0.130	0.54	0.73	0.38	0.29	0.137	0.131	0.210	0.104	0.086	0.101	0.076	0.047
R15	3.0	0.1 & 1.0	0.034 & 0.041	0.37	0.39	0.16	0.18	0.272	0.395	0.425	0.081	0.254	0.279	0.150	0.123
R16	3.0	0.1 & 1.0	0.052 & 0.062	0.48	0.53	0.31	0.12	0.220	0.276	0.298	0.128	0.169	0.223	0.124	0.072
R17	3.0	0.1 & 1.0	0.071 & 0.084	0.53	0.67	0.34	0.10	0.173	0.199	0.267	0.101	0.132	0.157	0.086	0.085
R18	3.0	0.1 & 1.0	0.090 & 0.107	0.58	0.75	0.35	0.19	0.144	0.154	0.233	0.087	0.108	0.130	0.074	0.061
R19	3.0	0.1 & 1.0	0.130 & 0.153	0.55	0.66	0.43	0.31	0.116	0.112	0.177	0.088	0.079	0.091	0.069	0.054
R20	3.0	0.1 & 1.0	0.149 & 0.176	0.43	0.56	0.41	0.32	0.107	0.087	0.139	0.109	0.063	0.068	0.066	0.052
R21	3.0	0.1 & 1.0	0.168 & 0.198	0.33	0.50	0.32	0.38	0.099	0.074	0.145	0.097	0.064	0.060	0.082	0.043
R22	3.0	0.1 & 1.0	0.186 & 0.219	0.40	0.49	0.50	0.43	0.086	0.069	0.133	0.076	0.056	0.050	0.054	0.050

During the past four years, however, seabed erodibility has been measured in over 100 sediment cores collected from Louisiana shelf and estuaries, and the findings were recently published in Xu et al. (2014), Lo et al. (2014) and Mickey et al. (2014). Thus the logical next step is to apply the measured erodibility parameters to better quantify critical shear stresses and

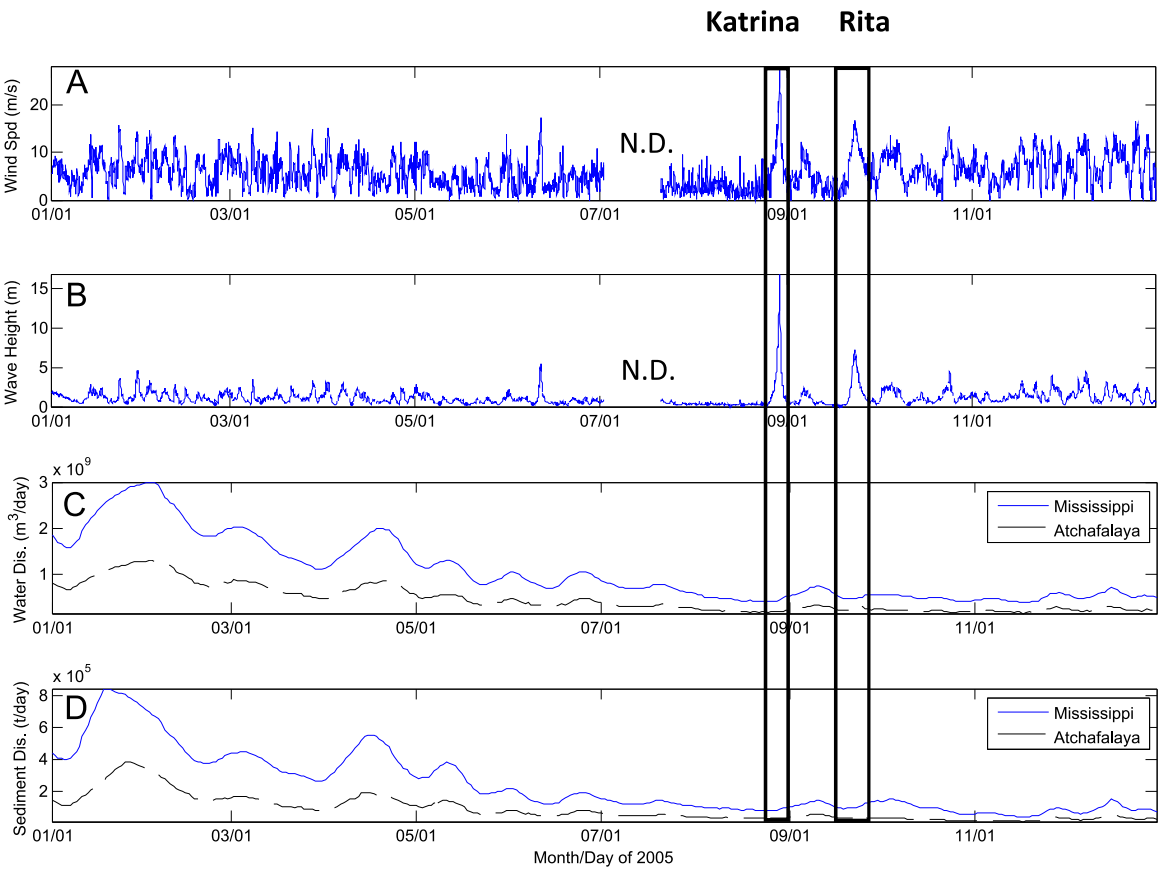

Fig. 5. (A) Wind speed (m/s) and (B) wave height (m) measured at NDBC station 42040. (C) and (D), water and sediment discharge from the Mississippi and Atchafalaya Rivers, measured at Tarbert Landing and Simmsport Stations, respectively. The periods during the passing of Hurricanes Katrina and Rita are highlighted in black columns. N. D.=No Data.

seabed erosional rates in a 3-D sediment transport model, and to apply that model for hurricane conditions to evaluate the role of hurricanes in resuspending and redistributing sediment.

In this study we strive to fill in the knowledge gap in hurricane sediment transport and study seabed erosion and deposition on Louisiana shelf before, during and after Hurricanes Katrina and Rita, and to evaluate our ability to make these calculations. Instead of using 2-D sediment transport models, we decided to use 3-D models to better characterize the bottom boundary layer dynamics in the lower water column. Specific objectives are to: (1) test the sensitivity and uncertainty of our 3-D sediment transport model to several key parameters, (2) study the horizontal pattern of maximum erosional depths both east and west of hurricane tracks, (3) compare the impacts from Hurricanes Katrina and Rita, and (4) identify knowledge gaps and make suggestions for future studies. We hope that our study serves as a stepping stone toward using realistic 3-D sediment transport models to investigate estuary-shelf sediment exchange during hurricanes in the future.

3. Methods

The study of Xu et al. (2011) was focused on fluvial sediment dispersal, but in this study we focus on seabed sediment resuspension under intense and rapidly changing (hourly) hurricane environments. Details of modeling methods are described later, but major improvements since our 2011 study are summarized here: (1) The wind field was changed from spatially-uniform to spatially-variable to better represent the hurricane conditions, such as the eyes of hurricanes; (2) Open ocean boundary conditions were changed from monthly climatology to daily conditions from a global model described below; (3) The number of vertical layers were increased from 20 to 30 to better represent the bottom boundary layer dynamics.

3.1. Parametric hurricane wind model

A parametric hurricane wind model (Hu et al., 2012a) based on the asymmetric Holland-type vortex models was adopted to create surface wind fields 10 m above sea surface. This wind model can resolve the asymmetric structure of hurricanes. Storm parameters were taken from the U.S. National Hurricane Center's best track data (http://www.nhc.noaa.gov/data/). The 6-hourly background winds from the National Centers for Environmental Prediction and National Center for Atmospheric Research Reanalysis were merged with the hurricane winds. This wind model has been validated on historical Gulf of Mexico hurricanes, including Katrina and Rita (Hu et al. 2012b).

3.2. Unstructured SWAN wave model

The SWAN (Simulating Waves Nearshore) model is a third-generation spectral wave model for nearshore applications (Booij et al., 1999). An unstructured version of SWAN was developed recently (Zijlema, 2010), allowing for tight coupling with the storm surge Advanced Circulation (ADCIRC) model (Dietrich et al., 2011a). In recent years the Coastal Protection and Restoration Authority (CPRA) of Louisiana adopted a mesh developed by the ADCIRC modeling team at University of North Carolina. This mesh is similar to South Louisiana (SL) 15 mesh that was used in Bunya et al. (2010) and SL16 mesh that was published in Dietrich et al. (2011b). This mesh has about 1 million nodes and 2 million

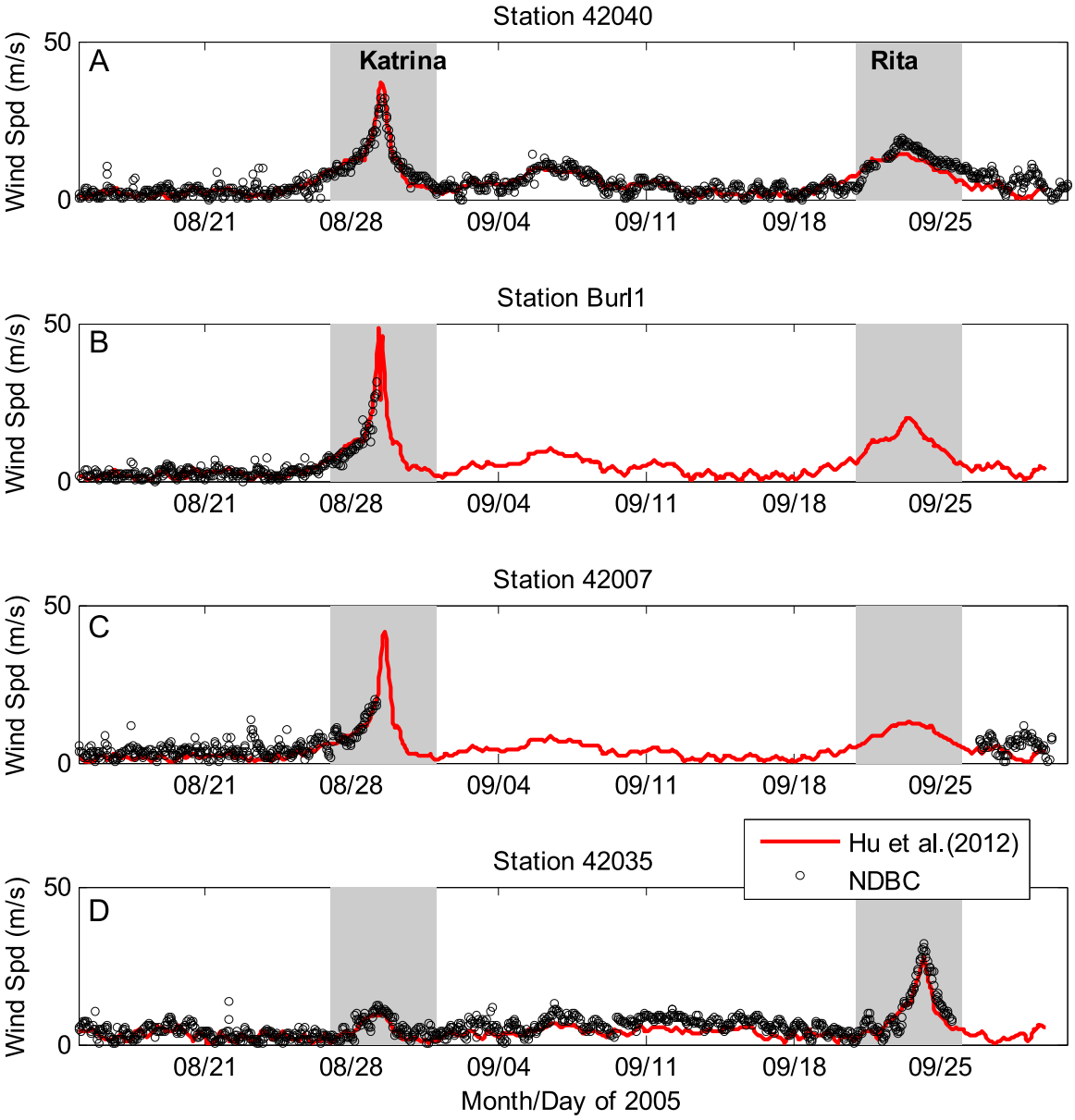

Fig. 6. Wind speed (m/s) comparisons between these measured at NDBC buoy stations and modeling data from Hu et al. (2012b).

elements, covering the entire Gulf of Mexico and northwestern part of the Atlantic Ocean. We used this mesh and ran SWAN-ADCIRC coupled model using non-stationary SWAN mode in spherical coordinates; 31 exponentially spaced frequencies from 0.0314 Hz to 0.5476 Hz with 36 evenly-spaced directions (10° resolution) for a time step of 60 min were used. Depth-limited wave breaking, steepness-limited wave breaking and bottom friction were captured in our model when waves move into the inner shelf. In addition, vegetation effects were included by using increased bottom friction in both SWAN wave and ADCIRC surge models. Wave parameters (height, direction and period) were interpolated on the ROMS model grid described below. Nearbed wave orbital velocity and period were then calculated using the method of Wiberg and Sherwood (2008). Wave parameters were validated for Hurricane Gustav (2008) along the Louisiana coast in Chen et al. (2011).

3.3. Hydrodynamic model

The hydrodynamic model was based on Regional Ocean Modeling System (ROMS; see Shchepetkin and McWilliams, 2005; Haidvogel et al., 2008). The curvilinear ROMS model grid used in this study (Fig. 2) was developed by Hetland and DiMarco (2008), and has been validated by Hetland and DiMarco (2012) and evaluated by Marta-Almeida et al. (2013). This model was also used by Xu et al. (2011), Fennel et al. (2011), among others. This model's grid cells varied from 2 to 10 km horizontally and a total of 30 vertical layers stretched using an S-coordinate were used. Both surface and bottom stretching parameters were set to be 3.0 and the critical depth was 3 m; this setting allowed higher vertical resolutions near both sea surface and sea bottom. The Mellor/Yamada Level-2.5 mixing closure and SSW_BBL bottom boundary layer defined in Warner et al. (2008) were used. The aforementioned parametric hurricane wind and unstructured SWAN wave models provided wind and wave inputs for this ROMS model. Open ocean boundary conditions were from global ocean circulation Hybrid Coordinate Ocean Model (HYCOM), updated every 24 h (Marta-Almeida et al., 2013). The ROMS model was initialized on February 1, 2005 and a time step of 20 s was used.

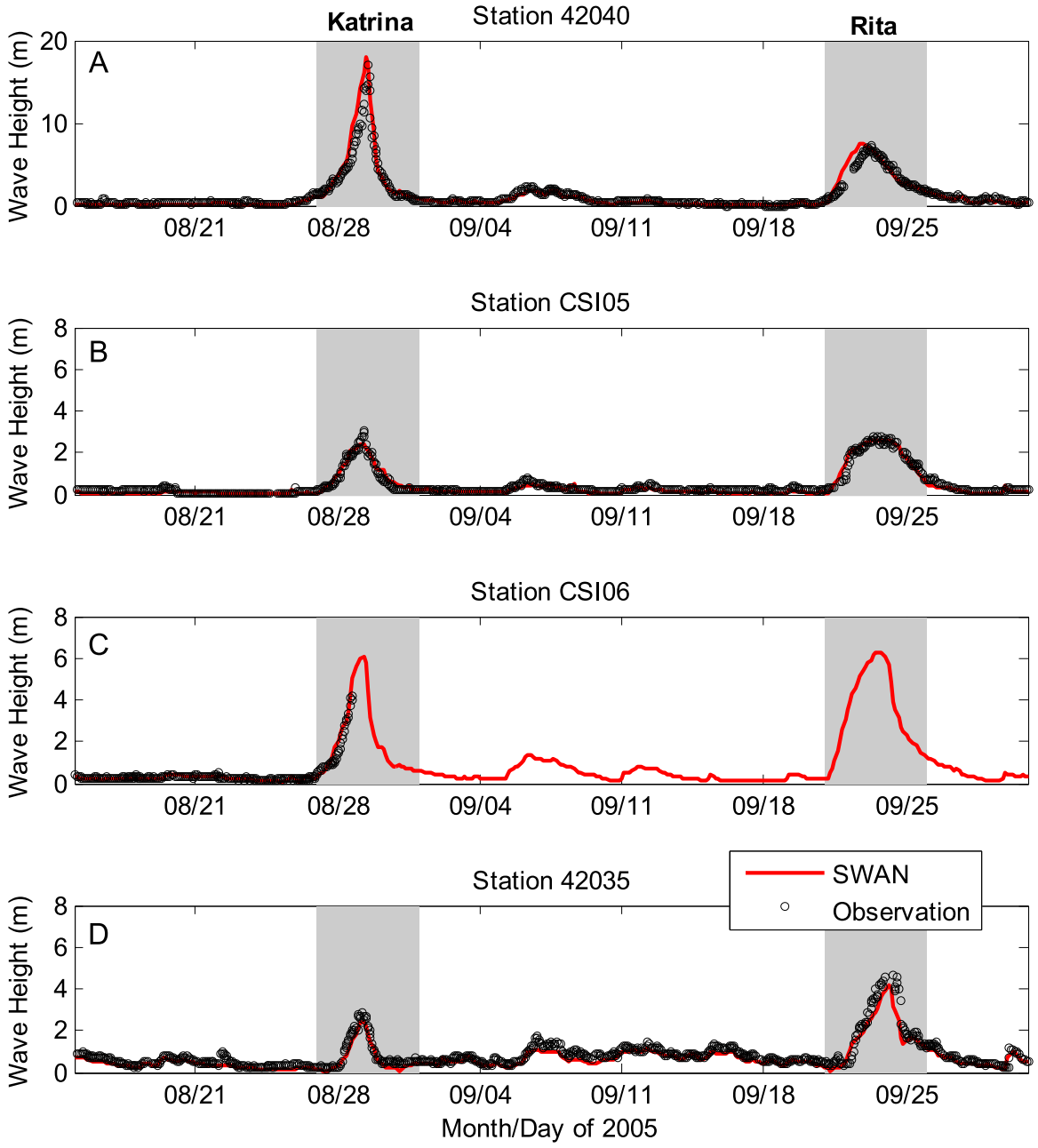

Fig. 7. Wave height (m) comparison of observational data from NDBC buoys and Louisiana State University's WAVCIS stations with modeling data from an un-structured SWAN model used in this study.

3.4. Sediment transport model

A total of six sediment tracers were used: two from the Mississippi River, two from the Atchafalaya River, and two from the seabed (see more details in Xu et al. (2011)). Mud percentages of over 50,000 historical surficial grain-size data from the usSEABED project (Buczkowski et al., 2006) were interpolated and assigned to the fine sediment tracer percentages on seabed, and sand percentages were assigned to the coarse tracer on seabed (Fig. 4). Sandy Trinity Shoal and Ship Shoal, for example, contained $<10\%$ of mud in the model domain (Fig. 4). Median grain sizes D_{50} of 63 and 250 μm were used for fine and coarse sediment tracers, respectively. A total of four seabed layers were used and each layer was 5 m thick, making a total of 20 m. These thick layers were used to prevent the removal of "total sediment reservoir" in sensitivity tests.

Seabed response to hurricanes can be conceptualized as the difference between competing *erosional* and *depositional* processes. The depositional flux is calculated as the product of near-bed sediment concentration and settling velocity W_s. The seabed surface erosional mass flux E_s in kg/m^2/s is calculated as:

$$E_s = E_0(1-\varnothing)\frac{\tau_b - \tau_{cr}}{\tau_{cr}} \quad (1)$$

where E_0 is seabed erosional rate parameter in kg/m^2/s, $\varnothing$ is porosity which is 0.8 in our model based on the measurements from Allison et al. (2007), τ_{cr} is critical shear stress in Pa, and τ_b is bed shear stress generated by waves and currents in Pa.

3.5. Sensitivity and uncertainty tests

Three parameters were considered in our sensitivity and uncertainty tests: settling velocities, erosional rate parameters and

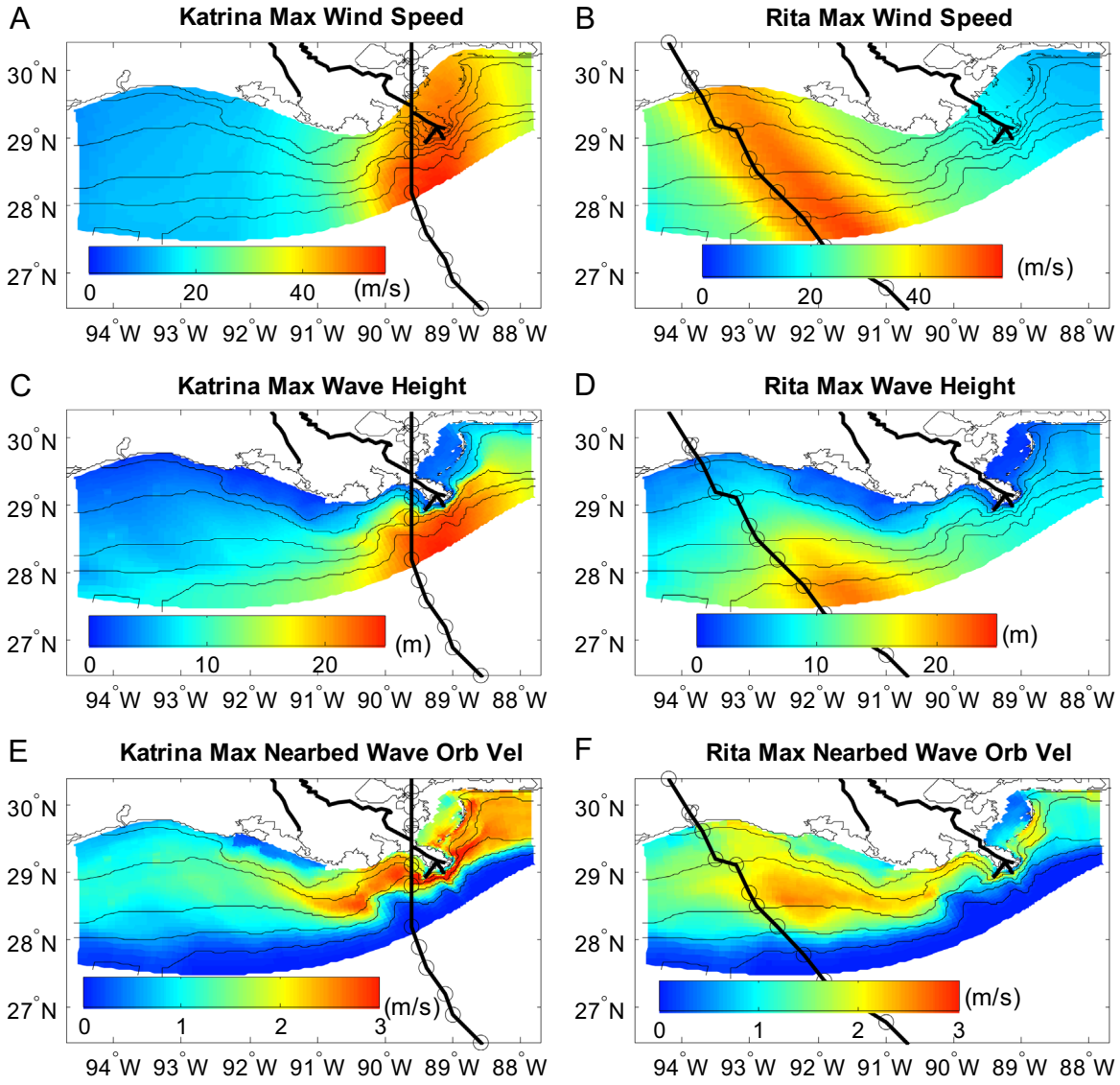

Fig. 8. Maximum wind speed (m/s), significant wave height (m), and significant nearbed wave orbital velocity (m/s) experienced during the passage of Hurricanes Katrina and Rita, respectively. Isobaths are at 10, 20, 50, 100 and 300 m.

critical shear stresses. We believe that these three parameters play very important roles in calculating erosional and depositional processes. Settling velocities and erosional rate parameters are used in sensitivity tests and critical shear stresses are used in uncertainty tests.

Firstly we did literature search and compared the parameters used in eight studies, all of which used ROMS sediment transport model (Table 1). There were no measurements of settling velocity in Louisiana Shelf, but Fox et al. (2004) reported a range of 0.1–10 mm/s of settling velocities in the muddy Po River Delta area. Considering the values used by other studies listed in Table 1, we chose 0.1 & 1.0, 0.5 & 5.0 and 1.0 & 10.0 mm/s for fine and coarse seabed tracers, respectively. Xu et al. (2014) reported seabed microcosm erosion data from Station 10B on Louisiana shelf (Fig. 2) and average erosional rate at the level of 0.45 Pa (the highest calibrated stress) was calculated to be $\sim 5.0 \times 10^{-5}$ kg/m^2/s. Unfortunately this level of shear stress was much smaller than the modeled peak shear stress of ~50 Pa, and the eroded upper mm to cm thick of sediment in Station 10B is quite different from dm to m thick of seabed scour in our study. This rate of 5.0×10^{-5} kg/m^2/s was used in our initial model runs, but was too low to generate thick post-hurricane deposit observed by Goni et al. (2007). Moriarty et al. (2014) used 0.1×10^{-4} and 4.5×10^{-4} kg/m^2/s for the energetic Waipaoa Shelf in New Zealand which were based on seabed microcosm erosion measurements from Kiker (2012); Miles et al. (2015) used 5.0×10^{-4} kg/m^2/s for Mid-Atlantic Bight during Hurricane Sandy. We chose four levels of erosional rate parameters at 0.5, 1.0, 5.0 and 10.0×10^{-4} kg/m^2/s respectively, comparable to the values used in past studies (Table 1). Fixed critical shear stresses of 0.11 and 0.13 Pa were used for fine and coarse seabed tracers in sensitivity tests, consistent with these in Xu et al. (2011).

Thus three sets of settling velocities and four levels of erosional rate parameters yielded a total of 12 model runs (R1–R12, Table 2). We calculated post-Rita deposit thicknesses and compared them with the measurements by Goni et al. (2007). Linear regressions were used, and slopes, intercepts and correlations were calculated. Arithmetic averages and standard deviations of post-Rita deposit thicknesses were also calculated at all 41 stations and compared with these of Goni et al. (2007).

The model runs were evaluated using the skill proposed by Willmott (1982):

Table 3
Slopes, intercepts and correlation coefficients (R) of linear regressions between post-Rita deposit thicknesses observed by Goni et al. (2007) and the modeled deposit thicknesses in R1–R22.

Run	Slope				Intercept (m)				Correlation coefficient R			
	All	West	Mid	East	All	West	Mid	East	All	West	Mid	East
R1	−0.016	0.033	0.177	0.363	0.035	0.016	0.037	0.018	0.046	0.142	0.370	0.413
R2	−0.033	0.091	0.091	0.316	0.063	0.029	0.083	0.045	0.053	0.179	0.105	0.243
R3	0.735	1.169	0.700	−1.422	0.131	0.051	0.243	0.209	0.383	0.596	0.344	0.486
R4	2.028	1.672	2.153	11.310	0.452	0.444	0.468	−0.018	0.354	0.392	0.356	0.616
R5	−0.013	0.001	0.021	0.012	0.006	0.002	0.005	0.006	0.167	0.052	0.214	0.051
R6	−0.074	0.000	0.131	0.106	0.026	0.004	0.007	0.030	0.183	0.004	0.535	0.074
R7	−0.197	0.017	0.044	0.105	0.069	0.012	0.092	0.056	0.259	0.080	0.041	0.054
R8	0.121	0.223	0.901	−0.989	0.086	0.053	0.108	0.126	0.093	0.182	0.493	0.500
R9	−0.006	0.001	0.021	0.004	0.003	0.001	0.001	0.004	0.111	0.131	0.454	0.022
R10	−0.060	0.003	0.058	−0.190	0.016	0.001	0.002	0.033	0.183	0.200	0.551	0.151
R11	−0.172	0.006	0.122	0.284	0.054	0.005	0.018	0.060	0.210	0.111	0.289	0.099
R12	−0.122	0.001	0.368	0.085	0.058	0.017	0.046	0.057	0.200	0.004	0.430	0.052
R13	0.059	0.277	0.129	0.611	0.096	0.040	0.128	0.069	0.074	0.419	0.113	0.357
R14	0.335	0.650	0.279	−0.257	0.108	0.042	0.193	0.118	0.278	0.548	0.212	0.142
R15	1.701	1.962	−0.451	−0.732	0.125	0.126	0.453	0.121	0.476	0.600	0.173	0.156
R16	1.239	1.661	0.870	−1.585	0.113	0.048	0.245	0.215	0.520	0.636	0.405	0.582
R17	0.726	1.114	0.530	−1.683	0.111	0.046	0.235	0.193	0.390	0.605	0.355	0.522
R18	0.580	0.964	0.296	−0.717	0.094	0.022	0.215	0.126	0.380	0.632	0.231	0.307
R19	0.286	0.498	0.315	0.003	0.092	0.044	0.158	0.088	0.258	0.470	0.265	0.001
R20	0.064	0.331	0.120	−0.036	0.102	0.041	0.132	0.111	0.072	0.419	0.104	0.018
R21	−0.030	0.224	−0.064	0.091	0.101	0.043	0.149	0.092	0.033	0.317	0.045	0.056
R22	0.075	0.217	0.253	0.448	0.079	0.039	0.118	0.051	0.096	0.368	0.269	0.234

$$skill = 1 - \frac{\sum_{i=1}^{N} |\eta_{mod} - \eta_{obs}|^2}{\sum_{i=1}^{N} \left(|\eta_{mod} - \bar{\eta_{obs}}| + |\eta_{obs} - \bar{\eta_{obs}}| \right)^2} \quad (2)$$

Where η_{obs} and η_{mod} are observational and modeling post-Rita deposit thicknesses, respectively, and $\bar{\eta_{obs}}$ is the corresponding average. Perfect agreement yields a skill of 1.0 whereas a complete disagreement gives a skill of 0. This skill method has been used by many studies, including the storm surge work by Zhong et al. (2010) and Ferreira et al. (2014). The model runs were also evaluated using Taylor Diagram based on second-order statistics including correlation, standard deviation and centered root-mean-square difference; this diagram does not provide information about overall biases, but solely characterizes the centered pattern error (Taylor, 2001).

Two erosional rate parameters of 2.0 and 3.0×10^{-4} kg/m^2/s were used in additional model runs R13 and R14 to get better modeling results. Since R14 produced the highest skill and best second-order statistics on Taylor Diagram, it was then defined as the "baseline" model run, which was later used in the uncertainty tests on critical shear stresses. In order to compare spatial responses to sensitivity tests, we also defined three areas: west (west of 91.8°W, including 15 stations; Atchafalaya River dispersal system), middle (between 91.8°W and 90.1°W, 9 stations; Louisiana shelf) and east (east of 90.1°W, 17 stations; Mississippi River dispersal system), as shown in Fig. 3.

Typically uncertainty analyses represent input uncertainty via random samples using the methods like Monte Carlo techniques (Clancy et al., 2010), but this approach is not practical for our computationally expensive 3-D coupled sediment transport model. Introduced by Wiener (1938), emulator-based approaches offer a computationally more efficient alternative. Thus for uncertainty analysis we adopted a polynomial chaos approximation method from Mattern et al. (2013), which was based on Wiener (1938) and Xiu and Karniadakis (2003). Mattern et al. (2013) and our study share the same mode grid, and they did extensive sensitivity and uncertainty analysis of hypoxia estimates using a ROMS biogeochemical model. With the help of this statistical emulator, we introduced the uncertainty of critical shear stresses using beta distribution and investigated the probability density function (PDF) of post-Rita deposit mass. In the scaled beta distribution, both α and β were set to be 12.375 and a standard deviation was assigned to be 0.2. We selected these parameters because the resulting distribution is similar to a normal distribution with equal mean and standard deviation, following the method of Mattern et al. (2013). One advantage of the beta distribution is that it is truncated and thus does not allow for scaling factors less than zero. Based on R14, our scaling factors on nine quadrature points (from 0.31 to 1.69) were used in uncertainty model runs R15–R22, as listed in Table 2. The probability distribution of post-Rita deposit mass was then calculated using 100 bins based on the interpolation method of Mattern et al. (2013).

4. Results

4.1. Winds, waves and discharge

In August 2005, the passage of Hurricane Katrina brought wind speeds that exceeded 20 m/s and waves that were 15 m tall (Fig. 5A and B). In August and September 2005 water and sediment discharge from the Mississippi and Atchafalaya Rivers were relatively low (Fig. 5C and D). Modeled wind speeds were compared with the values measured at both NDBC buoys and WAVCIS stations. The model reproduced wind speeds recorded at the four stations, and correctly represented the spatial structure; Stations 42040, 42007, and BURL-1 had higher speeds during Katrina while the station to the west (42035) had higher winds during Rita (Fig. 6). The modeled significant wave heights also showed good agreement with the wave measurements from NDBC buoys and WAVCIS stations (Fig. 7).

Maximum wind speeds, wave heights and near-bed wave orbital velocities experienced during both hurricanes are shown in Fig. 8. The bands of energetic winds estimated to the east of tracks were wider than those to the west of tracks (Fig. 8A and B). Wave heights increased to about 25 m south of the MRD during Hurricane Katrina (Fig. 8C), and reached about 20 m during Rita (Fig. 8D). Near-bed significant wave orbital velocities were highly associated with bathymetry and wave height, and estimated high

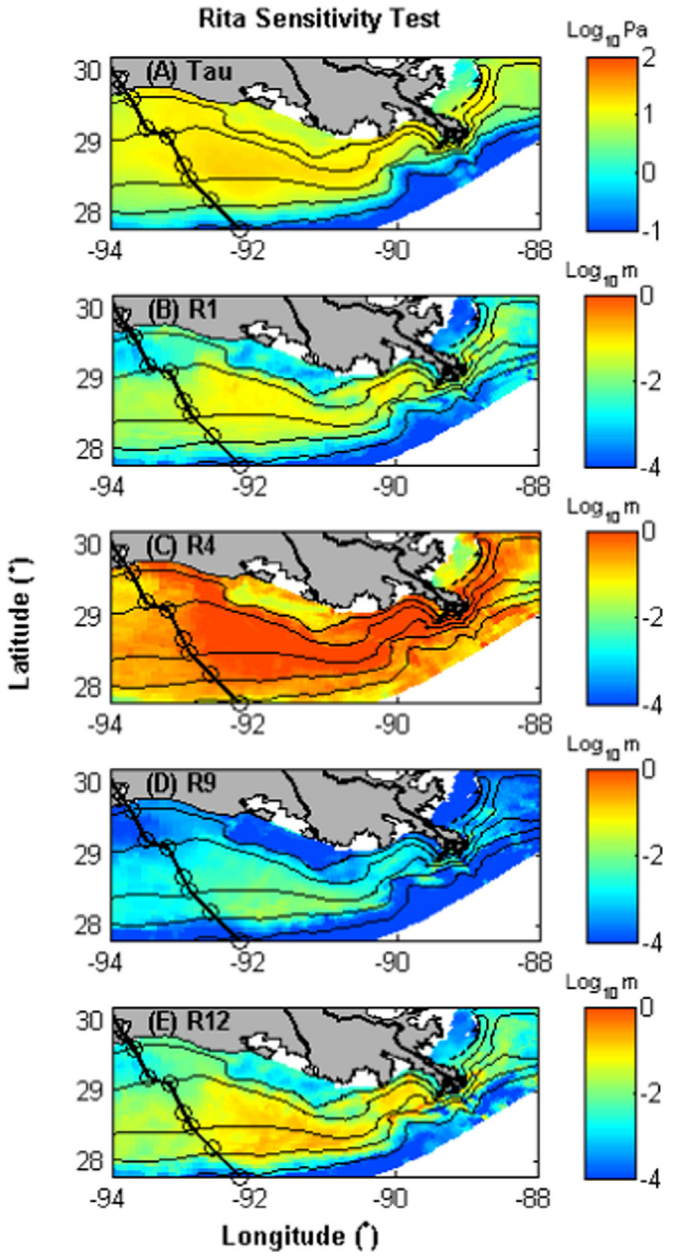

Fig. 9. (A) Maximum wave–current combined nearbed shear stresses ($\log_{10}$ Pa) experienced during the passage of Hurricane Rita. (B)–(E) Maximum erosional depths ($\log_{10}$ m) are for model runs R1, R4, R9 and R12. See Table 2 for input parameters used in these model runs. Black line and circles indicate Hurricane Rita's track. Isobaths are at 10, 20, 50, 100 and 300 m.

values were found between the 20- and 50-m isobaths (Fig. 8E and F).

4.2. Sensitivity tests

Skills, averages and standard deviations of all 41 stations as well as west, middle and eastern areas (defined in Fig. 3) for model sensitivity runs R1–R14 are shown in Table 2; slopes, intercepts and correlation coefficients are in Table 3. Maximum erosional depths during Hurricane Rita in R1, R4, R9 and R12 are shown in Fig. 9, along with the maximum wave–current bed stresses in Fig. 9A. Not surprisingly the erosional depths were smallest in R9 which assumed a low erosional rate parameter and high settling velocities; they were largest in R4, which assumed a high erosional rate parameter and low settling velocities. The spatial patterns of maximum erosional depths were similar to those calculated for the peak combined wave–current shear stresses (Fig. 9).

Of 14 model runs R1–R14, only R3, R4, R8, R13 and R14 generated positive slopes for entire study area ("All" in Table 3). R13 and R14 are closest to the 'observed' dot on Taylor Diagram (Fig. 10). Because of its best skill, R14 is defined as the baseline model run. West, middle and east areas responded to the changing inputs quite differently, as shown in Tables 2 and 3. The 'decoupled' responses in east and west areas seemed to lead to an overall poor skill and some negative slopes in multiple model runs (Tables 2 and 3).

4.3. Uncertainty tests

A total of 9 uncertainty tests (R14–R22) were performed, and the critical shear stresses of 0.11 and 0.13 Pa in the baseline model run R14 were multiplied by 9 levels of scaling factors: from 0.31 to 1.69 (Fig. 11A and Table 2). Modeled post-Rita deposit mass decreased with increased critical shear stresses (Fig. 11B). In model run R14, the estimated post-Rita deposit in the entire ROMS model domain was 5639 Mt; the PDF of post-Rita deposit showed an asymmetrical distribution, with a longer tail on the right side (Fig. 11C).

4.4. Hurricane sediment dynamics

Modeling results of R14 are used in this section to investigate sediment dynamics. During the peak of Hurricane Katrina, wind speeds exceeded 50 m/s and the strongest winds were formed east of the hurricane track (Fig. 12A). Tall waves of 20 m were generated south of the MRD. High bottom wave–current combined shear stresses, calculated as exceeding 30 Pa, were formed between the 10 and 50-m isobaths (Fig. 12C). During Hurricane Rita, the maximum wave height was 15 m, centered along the 50-m isobaths (Fig. 12B); high shear stresses were also produced between the 10 and 50-m isobaths (Fig. 12D).

Time series of wind speeds, shear stresses and seabed elevation changes were calculated for four stations along the 20-m isobaths, labeled Miss, AB5, 10B and 8C (Fig. 13). Of these four locations, Station Miss experienced the highest wave–current combined shear stress of 50 Pa and the deepest cut of ~1.5 m during Hurricane Katrina (Fig. 13). The influence of Hurricane Katrina decreased with the increased distance from hurricane track, as seen in the changes from Miss, AB5, 10B to 8C, from east to west (Fig. 13). Hurricane Rita influenced all four stations but there was a clear time lag of about 12 h between the westernmost station (8C) and three other stations (Fig. 13).

5. Discussion

This section synthesizes our results by evaluating the relationship between spatial patterns of sedimentation and storm track, summarizing the computed sediment budget, and suggesting how the sensitivity and uncertainty analysis may be of use in future studies. Additionally, we relate our study to some previous modeling efforts from the literature to evaluate hurricane-driven sediment transport.

5.1. Storm track and sediment transport

It has long been known that the largest winds for hurricanes that occur at the Northern Hemisphere are expected to be to the

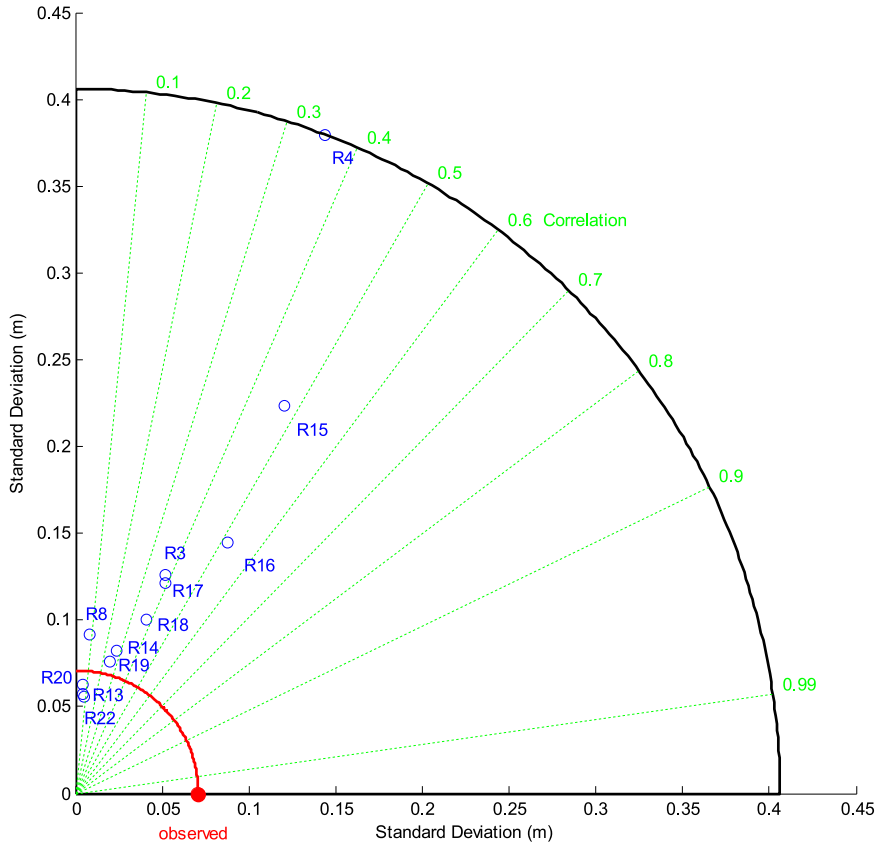

Fig. 10. Taylor diagram for model-observation comparisons of correlations and standard deviations of modeled post-Rita deposit (m).

right side of the storm, relative to the storm's motion. Likewise, waves generated by hurricanes are also typically largest in this sector (Wright et al. 2001). Previous numerical modeling studies have confirmed this. For example, Keen and Glenn (2002) employed a 3-D hydrodynamic model and reported that currents to the right side of Hurricane Andrew's track were larger than those to the left side. For Hurricane Katrina, the results of Keen et al. (2006) showed more intense wave energy to the right of the storm track. More recently, Miles et al. (2015) used a model similar to ours (ROMS – CSTMS) to represent Hurricane Sandy for the New Jersey shelf with the result that wave orbital velocities and sediment erosion peaked to the right side (in this case to the north) of the storm track.

Consistent with these patterns, in our model results there were wider bands of energetic winds, higher wind speeds east of the Hurricane Katrina and Rita tracks, which created larger waves there (Fig. 8). The wind patterns are as expected, because the hurricane winds flowed counterclockwise until landfall, after which wind speeds decelerated rapidly, especially in the western sector where winds blew seaward. The wave patterns likewise created larger wave orbital velocities and bed stresses to the right of the storm track, so that erosional depths were greatest there (Fig. 14). This was particularly true for Hurricane Rita, during which essentially all major sediment erosion and deposition were found east of the hurricane track (Fig. 14). The pattern of Katrina was less evident, probably due to the obstruction of the bird-foot shaped MRD.

During hurricane conditions, wave-induced shear stresses were much larger than those generated by currents so that sediment transport during hurricanes was highly dependent on wave dynamics. For both hurricanes, wave height peaked in fairly deep water ($>$ 100 m deep), while wave orbital velocities were highest in water depths of $\sim$20–50 m (Fig. 8). Wave energy dissipated quickly when water depths became shallower than 10–20 m, and wave orbital velocities and bed stresses also decreased dramatically in water deeper than 50 m because of the attenuation of nearbed wave orbital velocity with water depth (Fig. 8E and F). In response to these wave patterns, the "deepest cut" erosional bands on the seabed were mainly located between the 10- and 50-m isobaths (Fig. 14).

The hurricanes created localized areas of intensely energetic waves situated in open water, while wave height and orbital velocity decreased on the inner shelf. In contrast, during normal conditions or even large storms, the areas of most intense erosion may be more widespread and found in shallower water. For example, during average and fair weather conditions, our previous model results indicated that wave orbital velocity and bed stress continued to increase with decreasing water depth, into nearshore waters (Xu et al., 2011).

Estimated sediment fluxes during Katrina were high both east and west of the MRD, with net erosion in shallow water and net deposition in deeper water (Fig. 14E). The pattern of Rita was a bit mixed, but a northwestward transport can be clearly seen on the middle shelf (Fig. 14F). Sediment concentrations and fluxes were reduced above the sandy shoals south of Atchafalaya Bay due to the paucity of more easily suspendable fine-grained material there.

Hurricane wind speed and duration, air pressure, temperature gradients, and shelf topography all influenced the speed and direction of the currents that transported sediment (Turner et al., 2007). Being category four before making landfall, Hurricane Katrina moved along a nearly shelf-perpendicular track so that it spent little time ($\sim$48 h) on the continental shelf. As a result, Hurricane Katrina experienced rapid energy dissipation, causing

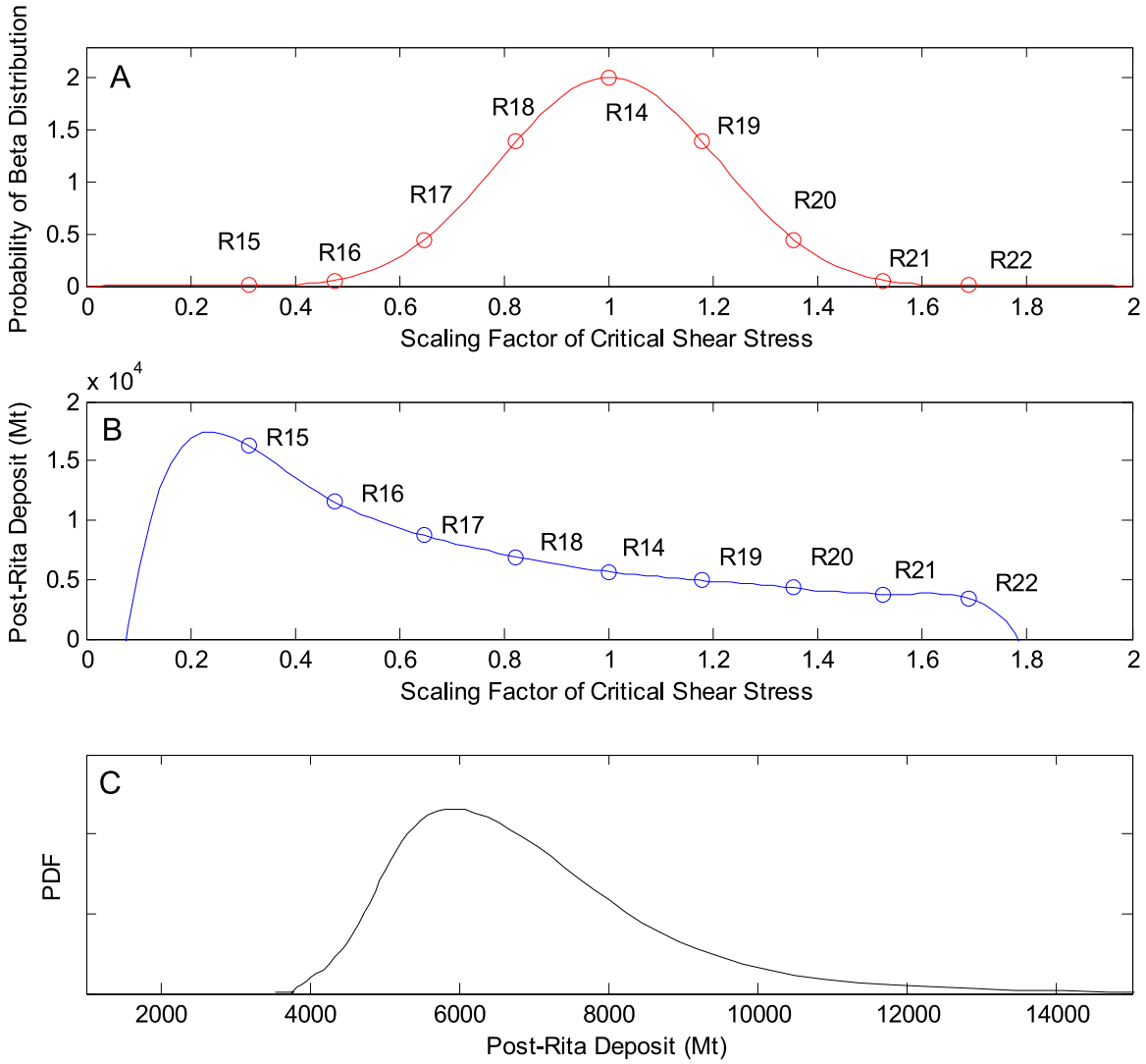

Fig. 11. (A) Probability of beta distribution and nine polynomial chaos quadrature points (circles). (B) Estimated post-Rita deposit (in Mt, Million tons, circles) for nine levels of scaling factors of critical shear stresses and the polynomial chaos approximation using 100 bins (line). (C) The probability density function (PDF) of estimated post-Rita deposit.

focused and intense disturbance surrounding the MRD. In contrast, Hurricane Rita, a category three, followed a more shelf-oblique track (Fig. 2), which kept it over the continental shelf for about 96 h. Its impact was more widespread, covering nearly the entire Louisiana coast, spanning the shelf from the Alabama–Mississippi border to the Louisiana–Texas border (Fig. 14B).

5.2. Sediment budget and contributing factors

We estimated the mass of the post-Rita deposit (Fig. 14D) for two model runs (R14 and R22), and calculated the mass for both the entire model domain and the study area sampled by Goni et al. (2007) (red polygon in Fig. 14D). We picked model run R22 because the average thicknesses of R22 and Goni et al. (2007) were both 0.086 m. Based on data from field and lab measurements by Goni et al. (2007), the observed post-Rita deposit in their study area accounted for 981 Mt of sediment. In model run R22, the deposits in Goni's study area and in the total model domain were 878 and 3416 Mt, respectively. In model run R14, the deposits in Goni's study area and the total model domain were 1404 and 5639 Mt, respectively. Compared to R14, R22 provided a better match for sediment mass, but showed less skill when compared to the actual deposits from sediment cores (Table 2). It is clear, however, both from the model runs and Goni et al.'s (2007) samples, that the total post-Rita deposit in the entire model domain was on the order of one billion tons, far exceeding the annual Mississippi River sediment discharge of 216 Mt/year. Note that, regardless of which model was used, a relatively small portion of the event bed mass actually lied in the area sampled by Goni et al. (2007) (Fig. 14D), illustrating the challenges in quantifying storm deposit masses via post-storm sampling.

5.3. Sensitivity and uncertainty

Over the range of values used for parameters within sensitivity tests R1–R14, the modeled average post-Rita deposit thicknesses varied by three orders of magnitudes, from 0.002 to 0.627 m over the entire model grid ("All" in Table 2). The settling velocities and erosional rate parameters were carefully selected for the baseline model run so that the observed and modeled values of deposit thickness were the same order of magnitude. The values used, $E_0 = 3 \times 10^{-4}$ kg/m^2/s, and w_s values of 0.1 and 1.0 mm/s, were

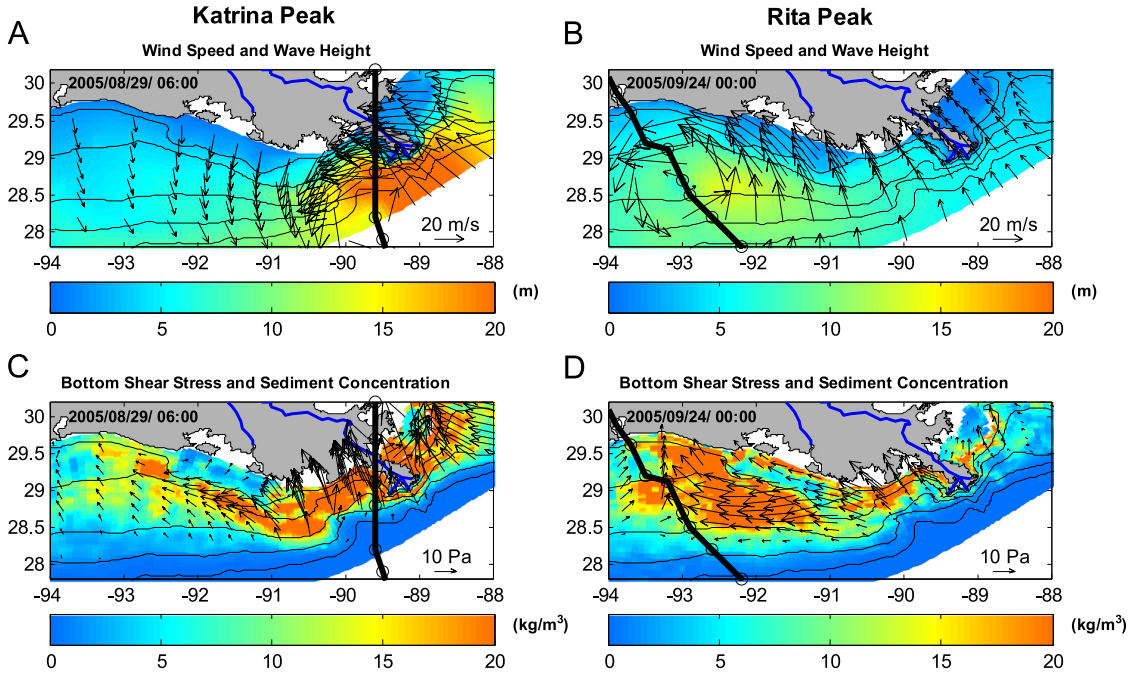

Fig. 12. (A) and (B), wind speed and direction (m/s, arrow) and significant wave height (m, color) during the peak of Hurricanes Katrina (at 2005/08/29 06:00 UTC) and Rita (at 2005/09/24 00:00 UTC), respectively. (C) and (D), bottom wave–current combined shear stress (Pa, arrow) and bottom water column sediment concentration (kg/m^3, color) during the peak of Hurricanes Katrina and Rita, respectively. Black line and circles indicate hurricane tracks. Isobaths are at 10, 20, 50, 100 and 300 m. Results are from model run R14. (For interpretation of the references to color in this figure legend, the reader is referred to the web version of this article.)

within the range of parameters used for other similar models (see Table 1). Unfortunately, field observations provide little guidance in specifying the hydrodynamic sediment properties for numerical sediment transport modeling in the northern Gulf of Mexico. Recent erodibility measurements provide some insight, and indicate that especially on the mid-shelf, the sediment is somewhat over consolidated, and that its erodibility varies in response to both physical and biological processes (Mickey et al., 2014; Xu et al., 2014; Briggs et al., 2015). For settling velocity, field observations provide even less guidance within the northern Gulf of Mexico. Until in-situ settling properties are measured there, numerical models will continue to treat settling velocity as a tuning parameter.

Next, we reevaluated our estimate of the Hurricane Rita deposit mass using an uncertainty analysis. The polynomial chaos expansion method provided a computationally more efficient alternative for propagating uncertainty in model inputs to their outputs. While it has been used within the Northern Gulf of Mexico for a biogeochemical model (Mattern et al., 2013), to our knowledge it has not been previously applied to a sediment transport problem. As illustrated in Fig. 11B, the estimated post-Rita deposit mass decreased by 13% from model run R14 to R19 when the critical shear stresses increased by 18%. In our uncertainty analyses, we assumed a standard deviation of 0.2 and beta distribution for the uncertainty of critical shear stresses, and then used nine model runs to evaluate the degree to which deposit mass varied over this range of critical shear stress. Fig. 11C shows that the mode of PDF of post-Rita deposit is around 6000 Mt but the distribution is positively skewed toward higher estimated deposit. Comparing variability in the sensitivity tests (R1–R14) of settling velocities and erosional rate parameters, there seem to be less overall variability in uncertainty tests (R15–R22) of shear stresses (Tables 2 and 3).

Additionally, critical shear stress represents a value that has both spatial and temporal variability, yet in the uncertainty analysis it was applied as a uniform and constant model parameter. In the future, more measurements of critical shear stress might be compiled to evaluate whether the beta distribution represents well the variability in critical shear stress during the conditions modeled. Additionally, the sensitivity tests showed that the deposit mass is sensitive to model parameters including the erosional rate parameter and settling velocity. Thus future studies might apply the polynomial uncertainty method to analyze variability for these parameters.

5.4. Ongoing studies and path forward

Our model used simple and fixed values of seabed critical shear stresses and erosional rates and neglected processes of consolidation and swelling for fine sediment. Xu et al. (2014) reported seabed erodibility curves of eroded mass vs. applied shear stress, and these curves can be applied in ROMS consolidation model, as described by Rinehimer et al. (2008) and done in a 3-D numerical model of the York River (Fall et al., 2014). The high resolution vertical seabed sorting can also be modeled in the new version of ROMS sediment transport model.

Additionally, while the consolidation model discussed above handles the variation in erodibility with depth in the seabed, Xu et al. (2014) found spatial variability in erodibility such that the seabed in deeper waters (like Mississippi Canyon, Fig. 2) was less erodible than that on the inner and middle shelves. Moriarty et al. (2014) report similar behavior for the Waipaoa shelf, New Zealand, and short of applying the full bed consolidation, they used a spatially varying erosional rate parameter so that E_0 decreased offshore. Thus spatial variability in seabed erodibility could also be added to the ROMS model using the method of Moriarty et al. (2014), but this does add another layer of model calibration to specify the manner in which erosion rate constant varies with

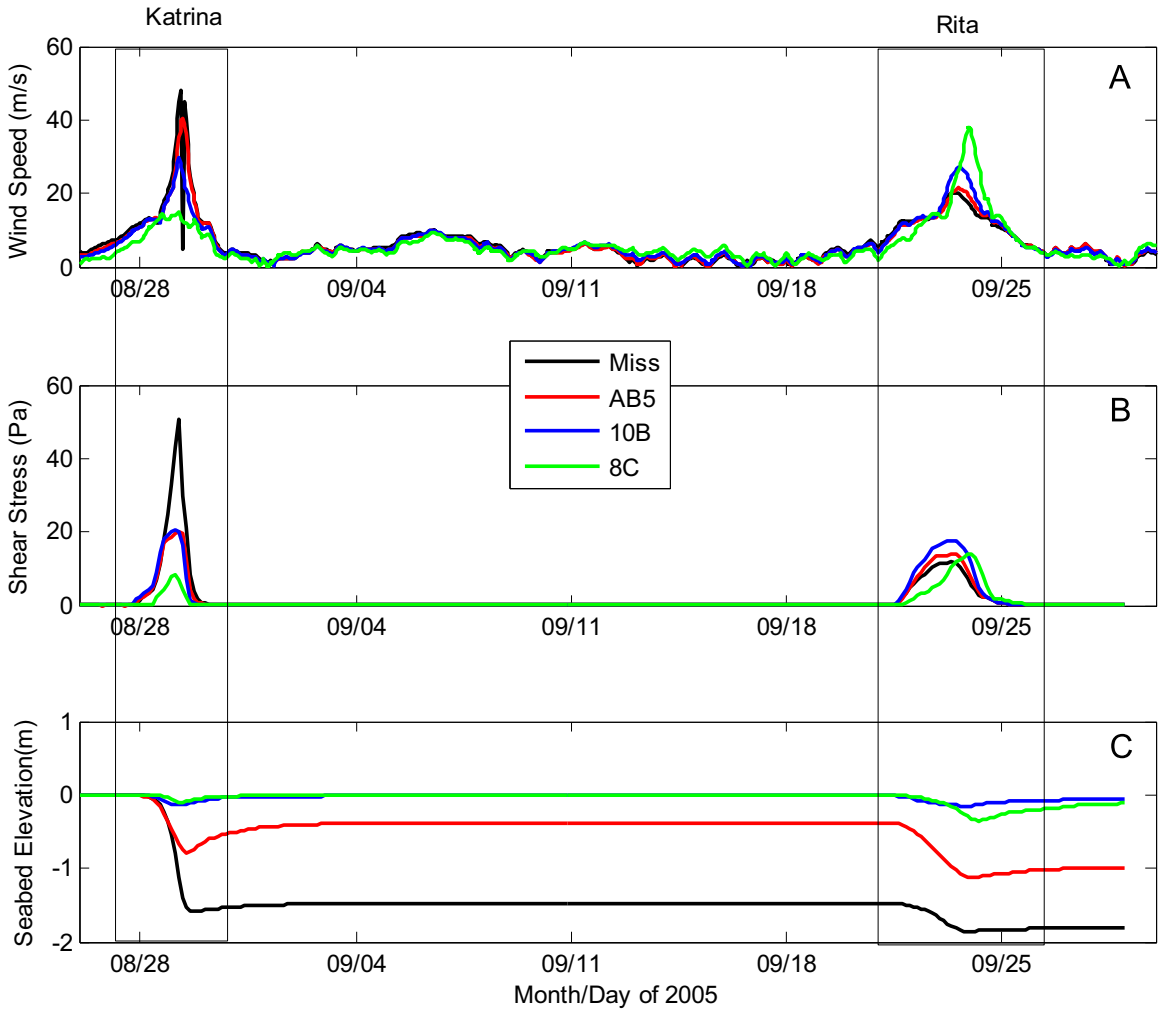

Fig. 13. Model estimated (A) wind speeds, (B) wave–current combined shear stresses (Pa) and (C) seabed elevation changes (m) at 4 selected stations (Miss, AB5, 10B and 8C) along the 20-m isobaths before and after Hurricanes Katrina and Rita. Results are from model run R14.

water depth or cross-shelf distance.

In this study the model estimated peak bed stresses of about 50 Pa, and suspended sediment concentrations in excess of 20 kg/m^3 under the extreme conditions during Hurricane Katrina. Rugged and robust optical and acoustic sensors are needed to measure high turbidity and energetic currents during hurricanes in the future.

6. Conclusions

Below are the major findings and conclusions in this study:

(1) Our coupled hydrodynamic – sediment transport model successfully represented extreme storm conditions, such as 50 m/s wind speeds and 25 m tall waves. The model estimated peak nearbed wave orbital velocities of 3 m/s that produced wave–current bed shear stresses of 50 Pa and over 1.5 m of seabed scour. The CSTMS sediment transport routine developed by Warner et al. (2008) proved to be robust to represent extreme and rapidly changing conditions.

(2) The maximum erosional depths were sensitive to model inputs, but spatial patterns for erosion mainly reflected hurricanes tracks, bed shear stresses, grain sizes and shelf bathymetry. The areas to the east of the hurricane tracks experienced stronger winds, taller waves and deeper erosion before landfall due to the counterclockwise wind movement, northward motion of the storms, and rapid weakening of wind energy. The largest waves, peak wave orbital velocities, and deepest erosion for both storms was within mid-continental shelf depths, because wave energy dissipated over the inner shelf.

(3) Hurricane Katrina took a fast and shoreline-normal path and caused intense and localized seabed disturbance along the eastern Louisiana shelf. Hurricane Rita, however, followed a shore-oblique path and its impact was widespread across the entire Louisiana shelf.

(4) Application of the Polynomial Chaos Uncertainty method allowed us to quantify the uncertainty in our estimates of the hurricane deposit mass that derive from difficulties in specifying the critical shear stress of the seabed. Comparing with variability in the sensitivity tests of settling velocities and erosional rate parameters, there seem to be less overall variability in uncertainty tests of shear stresses.

Acknowledgments

J.P. Walsh and D. Reide Corbett of East Carolina University

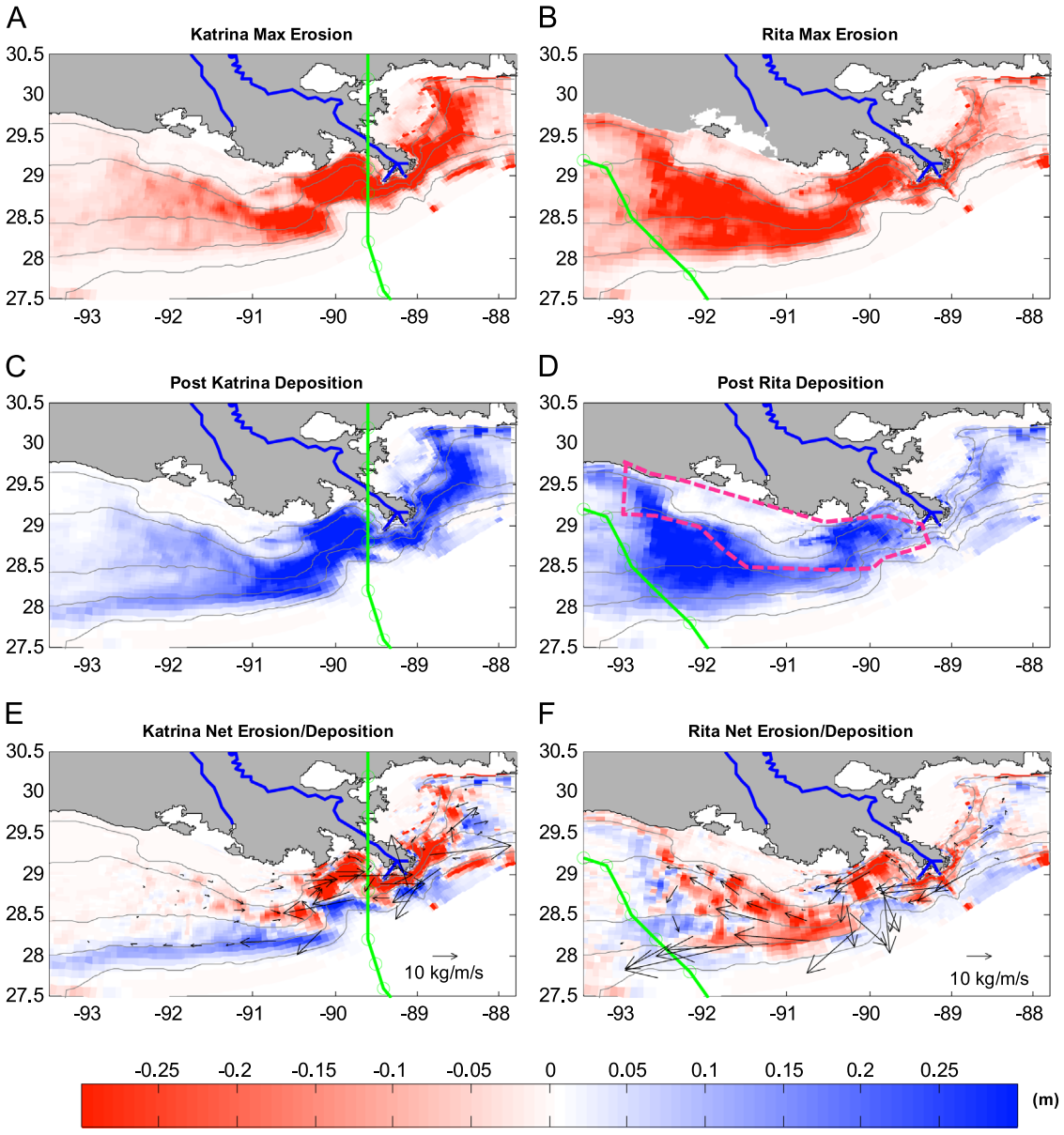

Fig. 14. (A) and (B), maximum erosional depth, (C) and (D), post-hurricane deposition and (E) and (F) net erosion/deposition calculated for Hurricanes Katrina and Rita, respectively. See Fig. 1 for the definitions of the above terms. Minus signs are added to maximum erosional depth so that the same colorbar can be used for all the panels. Green lines and circles indicate the hurricane tracks. Isobaths are at 10, 20, 50, 100 and 300 m. The dashed red polygon is for the budget interpolation of the study area of Goni et al. (2007). Arrows in (E) and (F) are depth-integrated and time-averaged sediment flux during the peaks of two hurricanes (about 3 day averages) in kg/m/s. Results are from model run R14. (For interpretation of the references to color in this figure legend, the reader is referred to the web version of this article.)

provided post-hurricane deposit data which were published in Goni et al. (2007), facilitating the comparison between the modeled and observed hurricane deposit. Paul Mattern (Dalhousie University) gave advice of uncertainty analysis and helped with polynomial chaos approximation. Martinho Marta-Almeida (Texas A&M University) helped with the access of boundary and climatology files used in the ROMS model. Chunyan Li of Louisiana State University provided WAVCIS data for model-observation comparison. Julia Moriarty of Virginia Institute of Marine Science provided suggestions on the use of the erosional rates in the ROMS model. We are grateful to three anonymous reviewers and the editors for their critical reviews and helpful suggestions. This study was supported by the U.S. National Oceanic and Atmospheric Administration (NA09NOS4780229, NGOMEX contribution #205). It is also contribution No. 3507 of the Virginia Institute of Marine Science, College of William & Mary.

References

Allison, M.A., Bianchi, T.S., McKee, B.A., Sampere, T.P., 2007. Carbon burial on river-dominated continental shelves: impact of historical changes in sediment loading adjacent to the Mississippi River. Geophys. Res. Lett. 34, L01606. http://dx.doi.org/10.1029/2006GL028362.

Bever, A.J., Harris, C.K., 2014. Storm and fair-weather driven sediment-transport within Poverty Bay, New Zealand, evaluated using coupled numerical models. Cont. Shelf Res. 86, 34–51. http://dx.doi.org/10.1016/j.csr.2013.07.012.

Bever, A.J., Harris, C.K., Sherwood, C.R., Signell, R.P., 2009. Deposition and flux of sediment from the Po River, Italy: an idealized and wintertime numerical modeling study. Mar. Geol. 260; , pp. 69–80.

Booij, N., Ris, R.C., Holthuijsen, L., 1999. A third-generation wave model for coastal regions, part 1, model description and validation. J. Geophys. Res. 104 (C4), 7649–7666.

Briggs, K.B., Cartwright, G., Friedrichs, C.T., Shivarudruppa, S., 2015. Biogenic effects on cohesive sediment erodibility resulting from recurring seasonal hypoxia on the Louisiana shelf. Cont. Shelf Res. 93, 17–26.

Buczkowski, B.J., Reid, J.A., Jenkins, C.J., Reid, J.M., Williams, S.J., Flocks, J.G., 2006. usSEABED: Gulf of Mexico and Caribbean (Puerto Rico and U.S. Virgin Islands)

offshore surficial sediment data release: U.S. Geological Survey Data Series 146, version 1.0. Available at: ⟨http://pubs.usgs.gov/ds/2006/146/⟩.
Bunya, S., et al., 2010. A high-resolution coupled riverine flow, tide, wind, wind wave, and storm surge model for Southern Louisiana and Mississippi. Part I: model development and validation. Mon. Weather Rev. 138, 345–377.
Chen, Q., Hu, K., Kennedy, A., 2011. Numerical modeling of observed hurricane waves in deep and shallow waters. Coast. Eng. Proc. 1 (32). http://dx.doi.org/10.9753/icce.v32.waves.30.
Clancy, D., Tanner, J.E., McWilliam, S., Spencer, M., 2010. Quantifying parameter uncertainty in a coral reef model using Metropolis-Coupled Markov Chain Monte Carlo. Ecol. Model. 221 (10), 1337–1347. http://dx.doi.org/10.1016/j.ecolmodel.2010.02.001.
Corbett, D.R., Walsh, J.P., Harris, C.K., Ogston, A.S., Orpin, A.R., 2014. Formation and preservation of sedimentary strata from coastal events: insights from measurements and modeling. Cont. Shelf Res. 86, 1–5.
Dietrich, J.C., et al., 2011a. Modeling hurricane waves and storm surge using integrally-coupled, scalable computations. Coast. Eng. 58 (1), 45–65.
Dietrich, J.C., et al., 2011b. Hurricane Gustav (2008) waves and storm surge: hindcast, synoptic analysis, and validation in Southern Louisiana. Mon. Weather Rev. 139, 2488–2522. http://dx.doi.org/10.1175/2011MWR3611.1.
Fall, K.A., Harris, C.K., Friedrichs, C.T., Rinehimer, J.P., Sherwood, C.R., 2014. Model behavior and sensitivity in an application of the cohesive bed component of the community sediment transport modeling system for the York River Estuary, VA. J. Mar. Sci. Eng. 2 (2), 413–436. http://dx.doi.org/10.3390/jmse2020413.
Fennel, K., Hetland, R., Fend, Y., DiMarco, S., 2011. A coupled physical–biological model of the Northern Gulf of Mexico shelf: model description, validation and analysis of phytoplankton variability. Biogeosci. Discuss. 8, 121–156.
Ferreira, C.M., Irish, J.L., Olivera, F., 2014. Uncertainty in hurricane surge simulation due to land cover specification. J. Geophys. Res. – Oceans 119, 1812–1827. http://dx.doi.org/10.1002/2013JC009604.
Fox, J.M., Hill, P.S., Milligan, T.G., Ogston, A.S., Boldrin, A., 2004. Floc fraction in the waters of the Po River prodelta. Cont. Shelf Res. 24 (15), 1699–1715.
Goff, J.A., Allison, M.A., Gulick, S.P.S., 2010. Offshore transport of sediment during cyclonic storms: Hurricane Ike (2008), Texas Gulf Coast, USA. Geology 38, 351–354.
Goni, M.A., Alleau, Y., Corbett, R., Walsh, J.P., Mallinson, D., Allison, M.A., Gordon, E., Petsch, S., Dellapenna, T.M., 2007. The effects of Hurricanes Katrina and Rita on the seabed of Louisiana shelf. Sediment. Rec. 5 (1), 4–9.
Goni, M.A., Gordon, E.S., Monacci, N.M., Clinton, R., Gisewhite, R., Allison, M.A., Kineke, G., 2006. The effect of Huricane Lili on the distribution of organic matter along the inner Louisiana shelf (Gulf of Mexico, USA). Cont. Shelf Res. 26, 2260–2280.
Haidvogel, D.B., Arango, H., Budgell, W.P., Cornuelle, B.D., Curchitser, E., Di Lorenzo, E., Fennel, K., Geyer, W.R., Hermann, A.J., Lanerolle, L., Levin, J., McWilliams, J.C., Miller, A.J., Moore, A.M., Powell, T.M., Shchepetkin, A.F., Sherwood, C.S., Signell, R.P., Warner, J.C., Wilkin, J., 2008. Ocean forecasting in terrain-following coordinates: formulation and skill assessment of the regional ocean modeling system. J. Comput. Phys. 227, 3595–3624.
Harris, C.K., Sherwood, C.R., Signell, R., Bever, A.J., Warner, J., 2008. Sediment dispersal in the northwestern Adriatic Sea. J. Geophys. Res. 113. http://dx.doi.org/10.1029/2006JC003868.
Hetland, R.D., DiMarco, S.F., 2008. How does the character of oxygen demand control the structure of hypoxia on the Texas–Louisiana continental shelf? J. Mar. Syst. 70, 49–62.
Hetland, R.D., DiMarco, S.F., 2012. Skill assessment of hydrodynamic model of circulation over the Texas–Louisiana continental shelf. Ocean. Model. 43–44, 49–62.
Hu, K., Chen, Q., Kimball, K.S., 2012a. Consistency in hurricane surface wind forecasting: an improved parametric model. Nat. Hazards 61, 1029–1050.
Hu, K., Chen, Q., Fitzpatrick, P.J., 2012b. Assessment of a parametric surface wind model for tropical cyclones in the Gulf of Mexico. In: Hickey, K. (Ed.), Advances in Hurricane Research – Modelling, Meteorology, Preparedness and Impacts. InTechhttp://dx.doi.org/10.5772/51288, ISBN 980-953-307-559-9.
Keen, T.R., Furukawa, Y., Bentley, S.J., Slingerland, R.L., Teague, W.J., Dykes, J.D., Rowley, C.D., 2006. Geological and oceanographic perspectives on event bed formation during Hurricane Katrina. Geophys. Res. Lett. 33, L23614. http://dx.doi.org/10.1029/2006GL027981.
Keen, T.R., Glenn, S.M., 2002. Predicting Bed Scour on the Continental Shelf during Hurricane Andrew. J. Waterw. Port. Coast. Ocean. Eng. 128, 249–257.
Kiker, J.M., 2012. Spatial and Temporal Variability in Surficial Seabed Character, Waipaoa River Margin, New Zealand (Master's thesis). East Carolina University, Greenville, NC, USA.
Knabb, R.D., Rhome, J.R., Brown, D.P., 2006. Tropical Cyclone Report, Hurricane Katrina, 23–30 August 2005, National Hurricane Center, pp 1–43.
Lo, E.L., Bentley, S.J., Xu, K., 2014. Experimental study of cohesive sediment consolidation and resuspension identifies approaches for coastal restoration: Lake Lery, Louisiana. GeoMar. Lett. 34 (6), 499–509. http://dx.doi.org/10.1007/s00367-014-0381-3.
Marta-Almeida, M., Hetland, R.D., Zhang, X., 2013. Evaluation of model nesting performance on the Texas–Louisiana continental shelf. J. Geophys. Res. – Oceans 118 (5), 2476–2491. http://dx.doi.org/10.1002/jgrc.20163.
Mattern, J.P., Fennel, K., Dowd, M., 2013. Sensitivity and uncertainty analysis of model hypoxia estimates for the Texas–Louisiana shelf. J. Geophys. Res. – Ocean. 118, 1316–1332. http://dx.doi.org/10.1002/jgrc.20130.
Mickey, R.C., Xu, K., Libes, S., Hill, J., 2014. Sediment texture, erodibility and, composition in the Northern Gulf of Mexico and their potential impacts on hypoxia formation. Ocean. Dyn. 65, 269–285. http://dx.doi.org/10.1007/s10236-014-0796-4.
Miles, T., Seroka, G., Kohut, J., Schofield, O., Glenn, S., 2015. Glider observations and modeling of sediment transport in Hurricane Sandy. J. Geophys. Res. – Ocean. 120, 1771–1791. http://dx.doi.org/10.1002/2014JC010474.
Moriarty, J.M., Harris, C.K., Hadfield, M.G., 2014. A hydrodynamic and sediment transport model for the Waipaoa Shelf, New Zealand: sensitivity of fluxes to spatially-varying erodibility and model nesting. J. Mar. Sci. Eng. 2, 336–369.
Neumann, C.J., Jarvinen, B.J., McAdie, C.J., Elms, J.D., 1993. Tropical Cyclones of the North Atlantic Ocean, 1871–1992. National Climatic Data Center, Asheville, North Carolina.
Rinehimer, J.P., Harris, C.K., Sherwood, C.R., Sanford, L.P., 2008. Estimating cohesive sediment erosion and consolidation in a muddy, tidally-dominated environment: model behavior and sensitivity. Estuarine and Coastal Modeling; Proceedings of the Tenth International Conference, Newport, RI. M.L. Spaulding, ed. pp 819-838. http://dx.doi.org/10.1061/40990(324)44.
Shchepetkin, A.F., McWilliams, J.C., 2005. The regional ocean modeling system (ROMS): a split-explicit, free-surface, topography-following-coordinate oceanic model. Ocean. Model. 9, 347–404. http://dx.doi.org/10.1016/j.ocemod.2004.08.002.
Stone, G.W., Grymes, J.M., Dingler, J.R., Pepper, D.A., 1997. Overview and significance of Hurricanes on the Louisiana Coast, USA. J. Coast. Res. 13 (3), 656–669.
Taylor, K.E., 2001. Summarizing multiple aspects of model performance in a single diagram. J. Geophys. Res. 106, 7183–7192.
Törnqvist, T.E., Paola, C., Parker, G., Liu, K., Mohrig, D., Holbrook, J.M., Twilley, R.R., 2007. Comment on Wetland Sedimentation from Hurricanes Katrina and Rita. Science 316, 201b.
Turner, R.E., Baustian, J.J., Swenson, E.M., Spicer, J.S., 2006. Wetland sedimentation from Hurricanes Katrina and Rita. Science 314, 449–452.
Turner, R.E., Baustian, J.J., Swenson, E.M., Spicer, J.S., 2007. Response to Comment on Wetland Sedimentation from Hurricanes Katrina and Rita. Science 316, 201c.
Tweel, A.W., Turner, R.E., 2012. Landscape-scale analysis of wetland sediment deposition from four tropical cyclone events. Plos ONE 7 (11), e50528. http://dx.doi.org/10.1371/journal.pone.0050528.
Walsh, J.P., et al., 2006. Mississippi delta mudflow activity and 2005 Gulf Hurricanes. Eos Trans. AGU 87 (44). http://dx.doi.org/10.1029/2006EO440002.
Warner, J.C., Armstrong, B., He, R., Zambon, J.B., 2010. Development of a coupled ocean–atmosphere–wave–sediment transport (COAWST) modeling system. Ocean. Model. 35 (3), 230–244.
Warner, J.C., Sherwood, C.R., Signell, R.P., Harris, C.K., Arango, H.G., 2008. Development of a three-dimensional, regional, coupled wave, current, and sediment-transport model. Comput. Geosci. 34, 1284–1306.
Wiberg, P.L., Sherwood, C.R., 2008. Calculating wave-generated bottom orbital velocities from surface–wave parameters. Comput. Geosci. 34, 1243–1262.
Wiener, N., 1938. The homogeneous chaos. Am. J. Math. 60 (4), 897–936. http://dx.doi.org/10.2307/2371268.
Willmott, C.J., 1982. Some comments on the evaluation of model performance. Bull. Am. Meteorol. Soc. 63, 1309–1313.
Wright, C.W., et al., 2001. Hurricane directional wave spectrum spatial variation in the open ocean. J. Phys. Ocean. 31 (8), 2472–2488.
Xiu, D., Karniadakis, G.E., 2003. Modeling uncertainty in flow simulations via generalized polynomial chaos. J. Comput. Phys. 187 (1), 137–167. http://dx.doi.org/10.1016/S0021-9991(03)00092-5.
Xu, K., Corbett, D.R., Walsh, J.P., Young, D., Briggs, K.B., Cartwright, G.M., Friedrichs, C.T., Harris, C.K., Mickey, R.C., Mitra, S., 2014. Seabed erodibility variations on the Louisiana continental shelf before and after the 2011 Mississippi River flood. Estuar. Coast. Shelf Sci. 149, 283–293. http://dx.doi.org/10.1016/j.ecss.2014.09.002.
Xu, K., Harris, C.K., Hetland, R.D., Kaihatu, J.M., 2011. Dispersal of Mississippi and Atchafalaya sediment on the Texas–Louisiana shelf: model estimates for the year 1993. Cont. Shelf Res. 31, 1558–1575. http://dx.doi.org/10.1016/j.csr.2011.05.008.
Xue, Z., He, R., Liu, J.P., Warner, J.C., 2012. Modeling transport and deposition of the Mekong River sediment. Cont. Shelf Res. 37 (1), 66–78.
Zhong, L., Li, M., Zhang, D., 2010. How do uncertainties in hurricane model forecasts affect storm surge predictions in a semi-enclosed bay? Estuar. Coast. Shelf Sci. 90, 61–72.
Zijlema, M., 2010. Computation of wind–wave spectra in coastal waters with SWAN on unstructured grids. Coast. Eng. 57 (3), 267–277.